

JGR Earth Surface

RESEARCH ARTICLE

10.1029/2021JF006294

Key Points:

- Remote-sensed channel network can enhance hydrological connectivity in numerical models
- We provide a simplified cost function method to determine the minimum channel depth in numerical models
- A minimum 2-m channel depth and a 4-grid width are required to simulate tidal propagation in wetland channels

Correspondence to:






X. Zhang,
zhangbu@bu.edu

Citation:

Zhang, X., Wright, K., Passalacqua, P., Simard, M., & Fagherazzi, S. (2022). Improving channel hydrological connectivity in coastal hydrodynamic models with remotely sensed channel networks. *Journal of Geophysical Research: Earth Surface*, 127, e2021JF006294. <https://doi.org/10.1029/2021JF006294>

Received 1 JUN 2021
Accepted 17 FEB 2022

Improving Channel Hydrological Connectivity in Coastal Hydrodynamic Models With Remotely Sensed Channel Networks

Xiaohe Zhang¹ , Kyle Wright² , Paola Passalacqua² , Marc Simard³ , and Sergio Fagherazzi¹ 

¹Department of Earth and Environment, Boston University, Boston, MA, USA, ²Department of Civil, Architectural, and Environmental Engineering, University of Texas at Austin, Austin, TX, USA, ³Jet Propulsion Laboratory, California Institute of Technology, Pasadena, CA, USA

Abstract Coastal wetlands are nourished by rivers and periodical tidal flows through complex, interconnected channels. However, in hydrodynamic models, channel dimensions with respect to model grid size and uncertainties in topography preclude the correct propagation of tidal and riverine signals. It is therefore crucial to enhance channel geomorphic connectivity and simplify sub-channel features based on remotely sensed networks for practical computational applications. Here, we utilize channel networks derived from diverse remote sensing imagery as a baseline to build a ~10 m resolution hydrodynamic model that covers the Wax Lake Delta and adjacent wetlands (~360 km²) in coastal Louisiana, USA. In this richly gauged system, intensive calibrations are conducted with 18 synchronous field-observations of water levels taken in 2016, and discharge data taken in 2021. We modify channel geometry, targeting realism in channel connectivity. The results show that a minimum channel depth of 2 m and a width of four grid elements (approximately 40 m) are required to enable a realistic tidal propagation in wetland channels. The optimal depth for tidal propagation can be determined by a simplified cost function method that evaluates the competition between flow travel time and alteration of the volume of the channels. The integration of high spatial-resolution models and remote sensing imagery provides a general framework to improve models performance in salt marshes, mangroves, deltaic wetlands, and tidal flats.

Plain Language Summary In hydrodynamic models, it is common to smooth topographic data to build the numerical grid. However, in coastal wetlands dissected by complex channel networks, this process would prevent an appropriate representation of channels for tidal propagation. This might lead to unreliable calculations of water fluxes between channels and wetlands. To address this issue, we modify channel geometry using remotely sensed data to enhance connectivity in simulations. Channel depth and width are determined by comparing model results to high-resolution field measurements. We develop a simplified cost function that can determine the optimal channel depth for tidal propagation without running computationally expensive simulations. Our results provide a framework to improve model performance of tidal flows along wetland channels by integrating numerical simulations, a simplified cost function, and remotely sensed channel networks.

1. Introduction

Coastal wetlands are natural buffer zones between land and ocean that provide protection from rising seas and storm surges (Fagherazzi et al., 2012, 2020; FitzGerald & Hughes, 2019; Schuersch et al., 2018). Sediment is essential for wetlands, because it promotes accretion that counteracts sea level rise (Donatelli et al., 2018; Ganju et al., 2017; Kirwan et al., 2016; Morris et al., 2002; Zhang et al., 2020). Unfortunately, as results of sediment starvation, loss of these valuable ecosystems is increasing worldwide. This is particularly true in large rivers, where damming has reduced the flux of material to the coast (Grill et al., 2015; Syvitski et al., 2009). In coastal wetlands, tidal and riverine channels control the transport of water and sediment (Fagherazzi, 2008; Friedrichs & Aubrey, 1988; Mariotti & Fagherazzi, 2012). The geometry of these networks of channels, such as branching and meandering characteristics, can directly determine the paths of sediment transport, the trapping efficiency of sediments within the system, and the nutrients delivery necessary for vegetation growth (Redfield, 1972; Rinaldo et al., 1999). Vegetation development can feed back to the morphological evolution of channels, leading to efficient channel networks (Kearney & Fagherazzi, 2016).

Despite the key functions of tidal channel networks, inappropriate representation of channel features in hydrodynamic models is common, and stems from two problems: (a) the coarse resolution of numerical models (Li & Hodges, 2019) and (b) inherent bathymetric errors in the channels (Cea & French, 2012; Torres & Styles, 2007; Wang et al., 2009). Coarse grids are often necessary due to computational constraints, as typical spatial domains of large connected wetlands are on the order of 100 km² and computational run times of 14 days to resolve spring-neap tidal cycles. However, coarse-resolution grids cannot resolve narrow creeks that are important for transport of flow and nutrients. Moreover, coarse models usually smooth channel depths, leading to channel discontinuity with unreliable calculations of water level and velocity along channels.

Bathymetric errors are often a result of stitching various data sets together, including digital terrain models (DTM) for land surface and sonar data for bathymetry. This often results in gaps in the data that must be interpolated over. Bathymetric surveys are very expensive and time-consuming, and are usually limited to the main channels where water depths are large enough to allow boating (Olliver et al., 2020; Shaw et al., 2016; Zhang et al., 2018). As a result, little information is available on the bathymetry of small channels that dissect the wetlands. Moreover, inevitable bathymetric errors occur in field measurements, data processing and data fusion to a uniform reference datum (Chust et al., 2010; List et al., 1997). All these problems affect the accurate representation of channels in quantitative wetland models.

The representation of channels in wetland models has been previously addressed in four different ways: (a) manual modification of bathymetry to regionally increase channel geomorphic connectivity, (b) addition of channel features detected by comparing high-resolution LiDAR data (e.g., 1 m) with the smoothed topography of coarse-grid models (e.g., ~30 m) (Hodges, 2015; Li & Hodges, 2019), (c) the development of subgrid models that solve shallow water equations on a coarse grid but incorporate high-resolution effects (e.g., friction) (Defina, 2000; Volp et al., 2013; Wu et al., 2016), and (d) optimization of mesh structures to capture subgrid topographic features (Bates et al., 2003).

Several studies have modeled wetlands with complex channel networks. Christensen et al. (2020) simulated water fluxes in the Wax Lake Delta, USA, with a refined grid size of 20 × 16 m. Despite the small grid size, they needed to manually modify the elevation in order to add a small creek between the main channel and one of the distributary channels. To represent narrow but hydrodynamically important blocking features in coastal models (e.g., levees), Hodges (2015) developed a method that automatically identifies levees in the fine-scale LIDAR topography of the Nueces River delta, Texas USA, and assigns the appropriate elevation values to a coarse-grid model. While the levee is a “positive feature” (elevation in fine-scale topography is higher than the smoothed topography in the coarse grid), similar methods have been tested for channels (e.g., “negative features”) to preserve the geometric connectivity of networks in shallow marsh systems (Li & Hodges, 2019). Although these methods can successfully enhance channel connectivity, the flow flux may be overestimated as the real subchannel width is narrower than a model grid cell.

Several coastal models utilize unstructured grids that are locally refined to follow channels and wetland boundaries (e.g., Christensen et al., 2020). To accurately model tides along the west coast of Britain, Jones and Davies (2005) tested a series of irregular unstructured grids (TELEMAC), and stressed the critical importance of local refinements in narrow channels such as the North Channel and Bristol Channel. These models better capture tidal propagation and hydrodynamics, but the process of mesh refinement is labor intensive and time consuming. More importantly, unstructured grids have elements of different dimensions that are not well suited for coupling with remote sensing data, which are typically available on squared grids. This problem is magnified when the study domain is very large; for example, it would be difficult to refine the mesh of a model spanning the entire Mississippi delta or the East Coast of the USA. A Cartesian grid also allows the coupling with ecological models built on a lattice, and is the preferred choice for climate models (e.g., Nijssen et al., 2001).

Therefore, there is a need to find a systematic way to modify a Cartesian mesh in order to capture tidal propagation in wetland channels. The goal of this paper is to address the inappropriate representation of channel networks and the inherent bathymetric errors at the same time, thus improving the hydrodynamic modeling of a wetland dissected by channels. We will determine what network of channels best reproduces water levels and tidal fluxes. Our main idea is to separately derive the channel network from remote sensing images, and then overlap it to the current model topography by assigning or modifying the depth of the channels. We will also explore what modifications of the channel network, specifically depth and width of channels, increase model performance.

This research provides a novel and systematic method to improve channel hydrological connectivity using freely available remote sensing imagery (e.g., Sentinel-2). Our approach will facilitate quantitative modeling of hydrodynamics in coastal systems with complex channel networks.

2. Study Area

The Wax Lake Delta (WLD) is a river-dominated delta located at the mouth of the Wax Lake Outlet (WLO), a channel artificially dredged in 1940s for the purpose of flood control (Figure 1a). As a diversion of the Atchafalaya River, the WLO conveys river flow and sediment into Atchafalaya Bay, facilitating the continuous growth of the WLD (Roberts et al., 2015; Shaw et al., 2013). Extensive shallow wetlands dissected by complex meandering channels are present at the two sides of the 300 m wide WLO (Carle et al., 2015). The wetlands are bounded by levees westward, and connect to the Atchafalaya Delta eastward. The Intracoastal Waterway, an artificial canal used for navigation, intersects with the WLO in the northern wetlands. Numerous small-scale branches and bifurcations develop along the primary channels (Figures 1b–1d).

The river discharge generally ranges from 2,500 m³/s to 5,000 m³/s with seasonal variations. The discharge is recorded at the Calumet Gauge (USGS 07381590) which is located about 20 km upstream of the delta. The system is fed by a mixed semidiurnal tide with a mean tidal range of 0.34 m. Despite the small tidal amplitude, tides dominate net flux exchanges and hydrological connectivity between channels and floodplain (Christensen et al., 2020; Hiatt & Passalacqua, 2015; Meselhe et al., 2021).

3. Data

3.1. Water Level and Discharge Data

Water level observations from 18 field sites are collected for model calibration, including eight stations (WL2–WL9) along the WLO temporarily deployed by the National Aeronautics and Space Administration (NASA), and 10 long-term sites of the Coastwide Reference Monitoring System (CRMS, <https://lacoast.gov/crms/>) in small creeks within the wetlands (Figure 1). Water surface elevation change was recorded every five minutes with millimeter accuracy at the WL2–WL9 stations using in situ pressure transducers during the NASA Pre-Delta-X Campaign on October 13–20, 2016 (Simard et al., 2020). At the CRMS sites, water levels are recorded hourly by a submersible data logger since 2010. These 18 sites cover the entire delta, quantifying water level gradients along the WLO (Figure 2a), and flow attenuation effects within the wetland channels (Figure 2b).

On 01 April 2021, acoustic doppler current profiler (Teledyne RiverPro ADCP) measurements of discharge were collected at five channel cross sections within the model domain (Figures 1g and 1h). Two or more replicate transects were taken and compared at each site, keeping the discharge measurements to differ by no more than 5% (Christensen et al., 2021).

3.2. Channel Networks Derived From Remote Sensing Data

We derived different maps of channel networks in the studied area from the National Wetland Inventory (NWI; <https://www.fws.gov/wetlands/>), Sentinel-2 classification maps (Thomas et al., 2019), and the Google Earth base map. The maps were processed into 10 m resolution binary imagery (Figure 3). The NWI classification data set from the US Fish and Wildlife Service is based on 1 m National Agriculture Imagery Program (NAIP) 4-band near infrared imagery, the National Elevation Model, and field measurements, in which they manually modified channels to increase connectivity. Considering the similarity between Sentinel-2 and NWI networks (Figure 3), we combine these two data set (S2&NWI) in the following analyses. The channel network extracted from the Google Earth base maps has numerous small-scale tributaries (Figure 3c). The channel width and centerline (skeleton) are calculated from the Google Earth map using RivGraph (Schwenk et al., 2020), a package for analyzing the morphologies and topologies of channel networks (Figure 4).

In this study, we are willing to modify ad hoc the bathymetry in order to achieve a more precise hydrodynamics. Note that because the bathymetry of the channels is often unknown or poorly constrained, to modify it with artificial values does not dramatically deteriorate the realism of the topography, but it increases the quality of the hydrodynamic results. The optimal channel network we want to derive is the one that better capture tidal

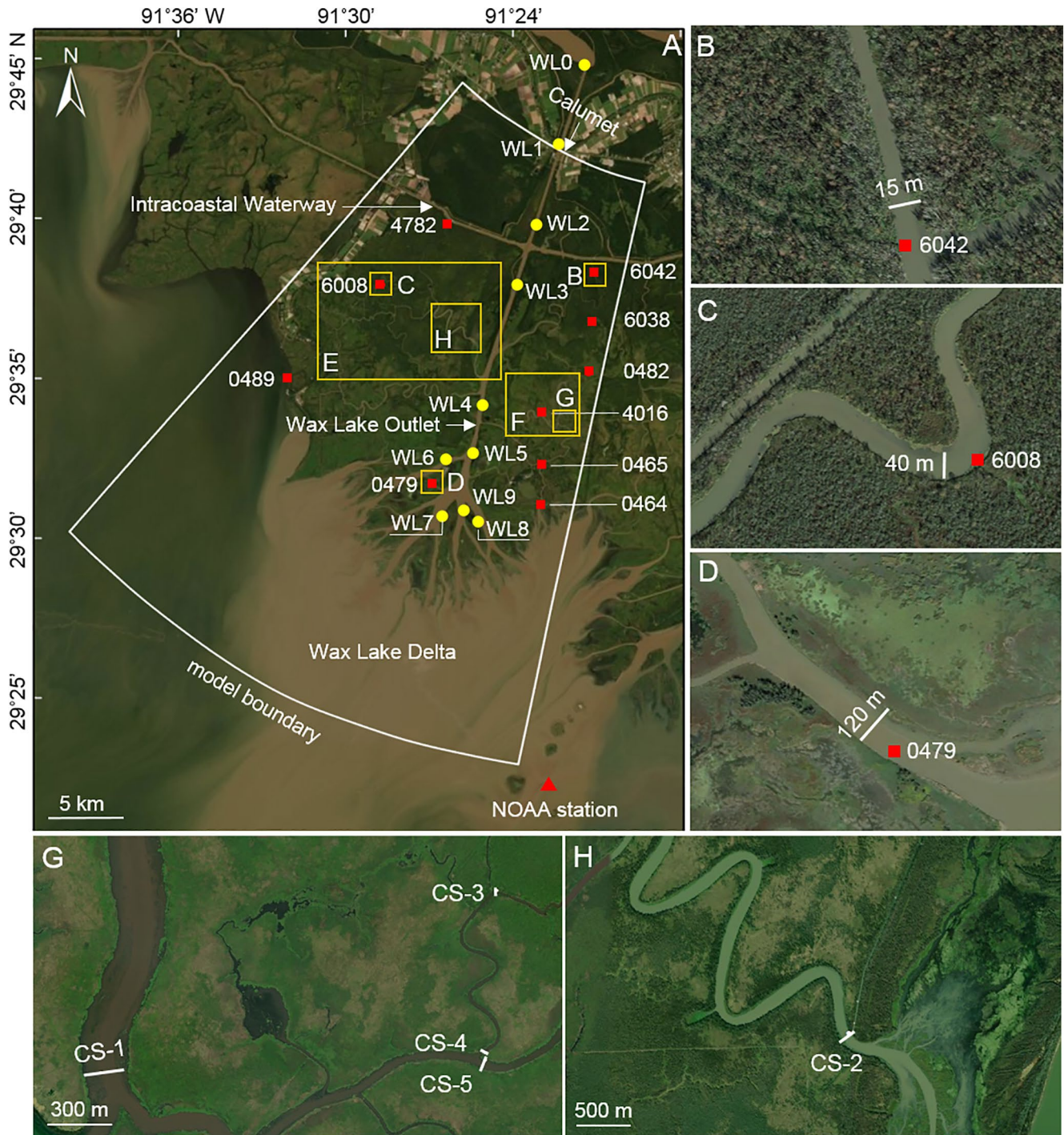


Figure 1. (a) Locations of Wax Lake Delta, model domain, and field measurement sites. Red squares are 10 sites of the Coastwide Reference Monitoring System (CRMS), and yellow dots are 10 water level gauges employed by NASA in 2016 (Simard et al., 2020). (b)–(d) Zoomed maps of channels adjacent to CRMS-6042, 6008, and 0479 sites respectively. (e), (f) Locations of subdomains for analysis in Figures 6 and 7 (g), (h) Locations of field measurements of discharge at five cross sections.

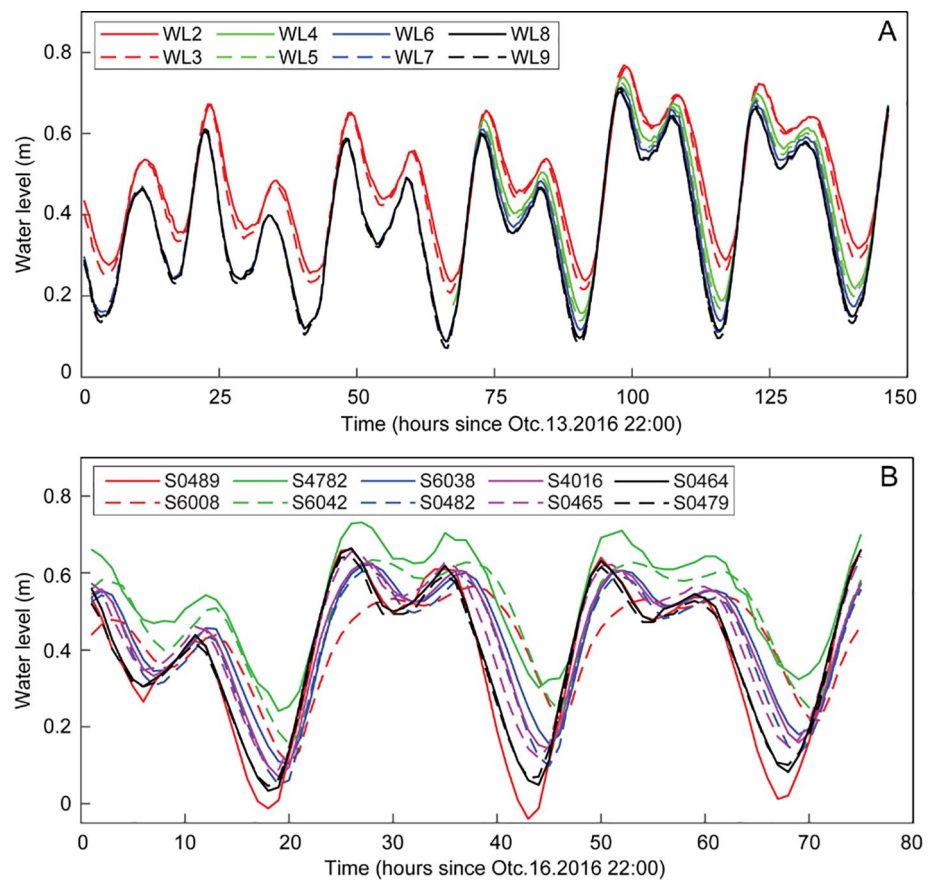


Figure 2. (a) Water-level measurements on October 13–20, 2016 at gauges WL2–WL9 along the Wax Lake Outlet, and (b) at 10 sites of the Coastwide Reference Monitoring System in wetland channels (see locations in Figure 1).

propagation in the creeks, and therefore it is the network that better represents water levels and discharge in the tidal channels.

4. Model Setup

Hydrodynamics were simulated using a high-resolution ($\sim 10 \times 10$ m) 2-D Delft3D FLOW model (Lesser et al., 2004). The model domain is discretized by a Cartesian grid of 2,600 by 1,700 cells, covering the entire delta and the upstream wetlands until the Calumet Gauge station (USGS 07381590, Figure 5), with higher resolution over the portion of the wetlands. The model topography is a 10 m seamless DTM composed of LiDAR datasets, sonar transects in channels, and bathymetric elevations derived from diverse source data and referred

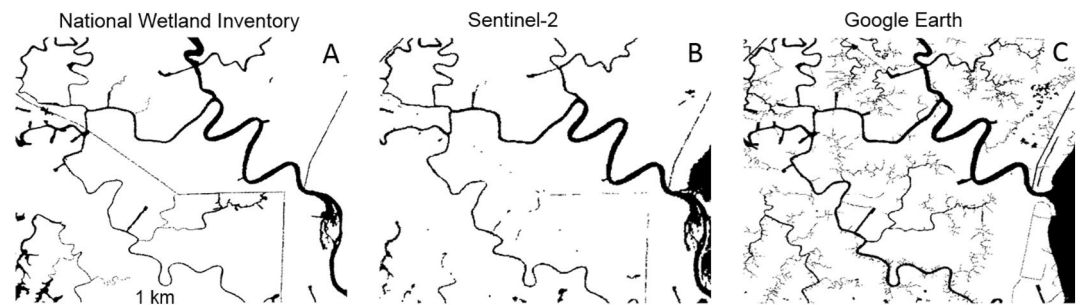


Figure 3. A subset of wetland channel networks (Figure 1e) at 10 m spatial resolution derived from (a) National Wetland Inventory, (b) Sentinel-2 imagery, and (c) Google Earth map. The black color indicates channels with water.

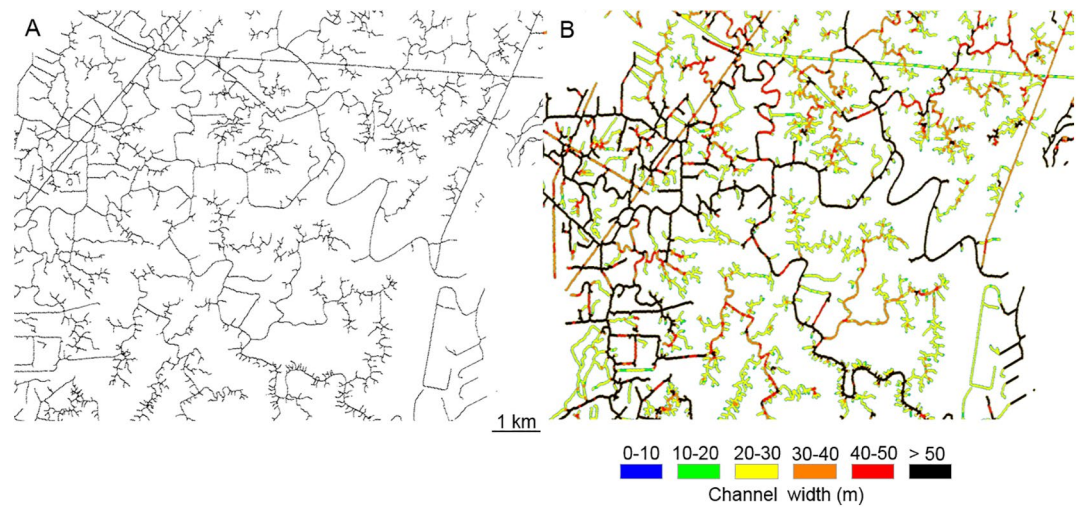


Figure 4. (a) Channel centerlines and (b) channel widths in a subset of the Wax Lake Delta wetlands derived from Google Earth.

to the NAVD88 vertical datum (Denbina et al., 2020). The wetland surface was derived from publicly available LiDAR data collected in 2015 (USGS 3-D Elevation Program). For the channels where we had no bathymetry (particularly the small channels), the channel width is estimated as the local maximum distance to LiDAR land points. The channel depth was set as 1/30 of channel width, based on the few surveys of tidal channels in the area (Denbina et al., 2020). For channels with width greater than 150 m, we relied on available bathymetric data. The

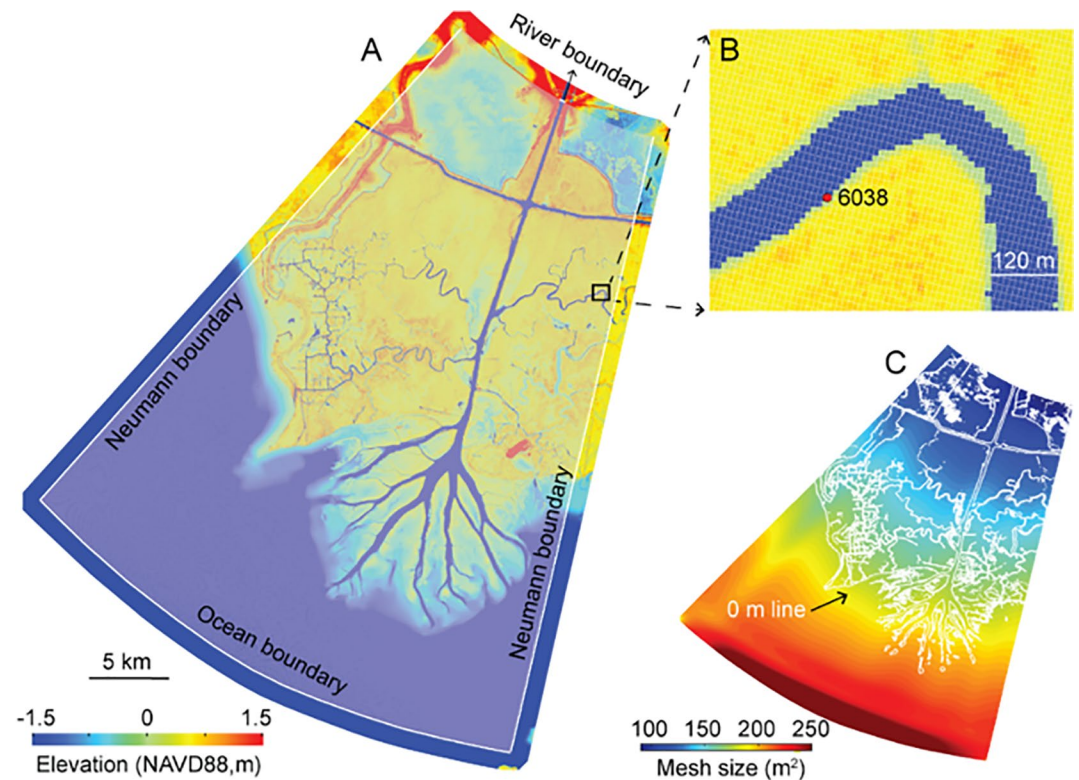


Figure 5. (a) Model setup and elevation data. (b) Zoomed map at site Coastwide Reference Monitoring System (CRMS)-6038 with model mesh. (c) Size of the mesh in the domain. Note the mesh is Cartesian and curvilinear with spatially varying size.

bank elevation was derived by linearly interpolating between the channel depth and the closest land elevation (which was derived from the USGS LiDAR DEM). The banks are 10 m wide at each side of the channel.

For boundary conditions, river discharge recorded at the Calumet Gauge station (U.S. Geological Survey, 2016) was specified as the upstream boundary, and hourly water levels recorded at the NOAA Amerada Pass station (NOAA 8764227; CO-OPS, 2018) as the ocean boundary (Figure 1a). The hourly wind conditions measured at the same NOAA station are uniformly prescribed across the model domain. The levees at the western boundary of the wetlands are represented by thin dam features in the model, thus accounting for the blocking effect.

The bed roughness is defined based on a 10 m Sentinel-2 classification map (Thomas et al., 2019) and a look-up table for the Chezy's coefficient: ocean (60 m^{1/2}/s), channel water (55 m^{1/2}/s), shoals (45 m^{1/2}/s), marsh (35 m^{1/2}/s), and forest (8 m^{1/2}/s) (Chow, 1959; Straatsma & Baptist, 2008). The simulation period is from 10 October 2016 at 00:00 to 20 October 2016 at 00:00, and a time step of 10s is adopted to satisfy all stability criteria for the parallel computation. To test the sensitivity of flow discharge to modifications of channel geometry, we set up another model for the simulation period from 25 March 2021 at 00:00 to 01 April 2021 at 00:00.

The Nash-Sutcliffe model efficiency (ME), root mean square error (RMSE) between the model (M) and field data (D) are used to evaluate model performance:

$$ME = 1 - \frac{\sum (D - M)^2}{\sum (D - \bar{D})^2}, RMSE = \sqrt{\sum \frac{(D - M)^2}{n}}, \quad (1)$$

where n is the number of observations. The value of ME represents the model performance: excellent when $ME > 0.65$; very good for $0.5 < ME < 0.65$; good for $0.2 < ME < 0.5$; poor for $ME < 0.2$ (Allen et al., 2007).

5. Experimental Design

In the initial topography (Figure 6a), a large number of channels are not well represented, including the Wax Lake entrance. In several channels, an unrealistic bathymetry shallower than 1 m is present. Instead of modifying the channel depths and widths locally by hand, we modify the channel depth and width using channel network maps with different accuracy derived from a combination of Sentinel-2 and NWI (S2&NWI) data, Google Earth maps, and channel centerline skeleton (Figures 3 and 4). We design a series of scenarios and test the sensitivity of tidal propagation to variations of channel depths (Table 1) and widths (Table 2).

To avoid an overestimation of the tidal prism (cumulative discharge within one tidal cycle) after modifying the channel geometry, an automatic simplification method is adopted to remove the small-scale channel branches of the initial network. The optimal scenario is determined by comparing the modeled water levels and discharge to measurements at the 23 observation sites.

5.1. Modification of Channels Depth

Channels in the network maps of Figure 6 with elevation <1 m (NAVD88) are deepened. The threshold of 1 m is determined by the fact that most small-scale creeks are deeper than 1 m. The sensitivity of different thresholds is also tested. Based on the S2&NWI channels, 12 scenarios are designed by lowering the channel depths from 0.5 to 10 m (M01–M13). For the Google Earth derived channels (name as “GE channels”) and the channel centerline skeleton, five scenarios are designed with a depth increase of 0.5 m, 1 m, 1.5 m, 2 m, and 3 m respectively (Table 1). The range of depth modifications are based on cross-sectional bathymetric surveys of wide channels (>100 m wide) and selected narrow channels (approximately 10 m wide) in 2021 (Christensen et al., 2021).

The process of channel depth modification using the S2&NWI network is illustrated in Figure 6. A modified DTM is obtained by incrementally deepening the channels derived from the S2&NWI network to recreate the scenarios in Table 1. Compared to the initial DTM, the modified DTM has an improved channel connectivity with a more realistic bathymetry >2 m (Figures 6a and 6c). Narrow artificial canals (straights lines in Figure 3b) are not well represented in the 10 m resolution of the Sentinel-2 imagery (Figure 6b). In order to avoid an over-carving of channel depths, we design a comparative scenario by only deepening channel centerline (three model grids) rather than the entire channel area (Figure 7).

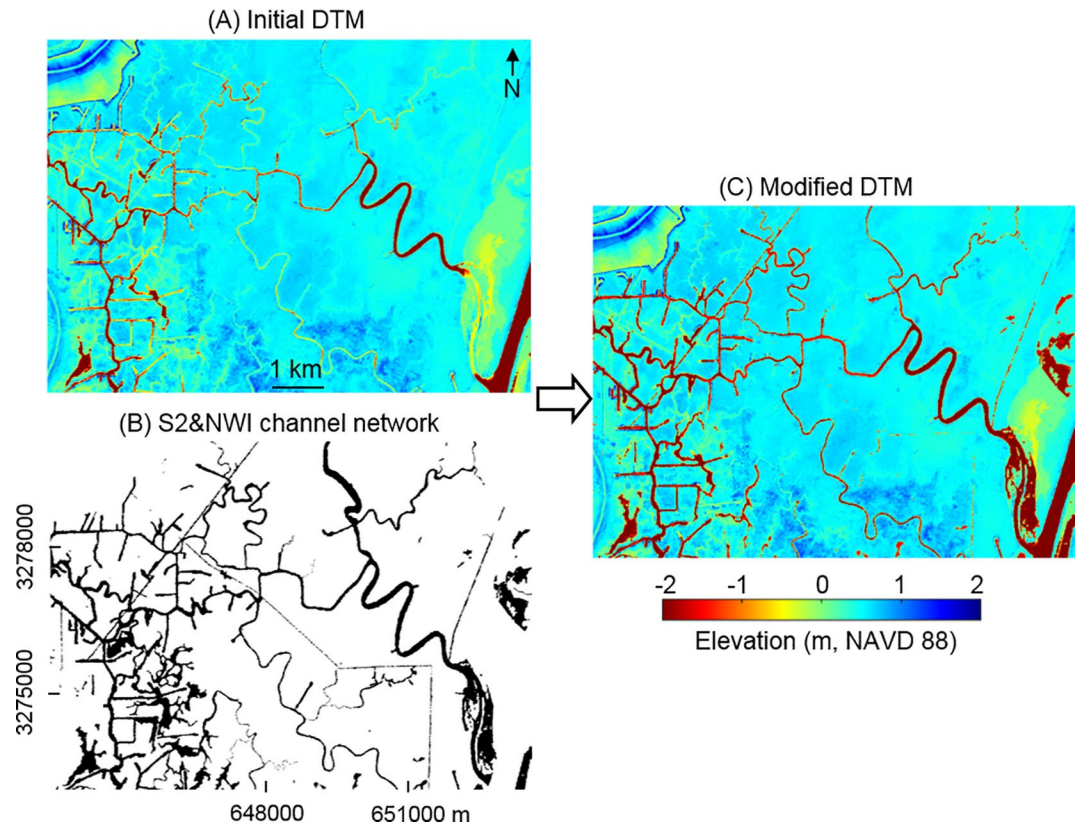


Figure 6. (a) Initial digital terrain model (DTM) of the subdomain E in Figure 1. (b) A Sentinel-2 Imagery & National Wetland Inventory (NWI) 10 m channel network derived by a combination of Sentinel-2 classification map (Thomas et al., 2019) and NWI channels (c) Modified DTM obtained by lowering by 2 m the depths of the channels derived from (b).

5.2. Modification of Channels Width

For channels with widths narrower or comparable to the model grid size, increasing channel depths may not improve channel connectivity. The blocking effect and the poor representation of the wetting and drying process will lead to unrealistic flow computation. In addition, it is impossible to have a correct tidal signal in secondary channels if primary channels are blocked. Therefore, we designed six scenarios by increasing channels width by 1, 2, and 3 cells (20 m, 40, and 60 m) before the channel depths are modified (C1, C2, and C3) and after the depths are modified (C4, C5, and C6) (Table 2, Figure 8). To be specific, in the grid the channels are expanded by one pixel at each side to represent the 20 m widening, and the bathymetry of the new channel pixel is updated by averaging the bathymetry of the nearby channel pixels. The values of bed roughness in the new channel pixels are

Table 1
Model Scenarios Obtained by Modifying the Depths of the Channels Derived From Sentinel-2 Imagery & National Wetland Inventory (S2&NWI; M01–M13), Google Earth Map (G01–G05), and Channel Centerline Skeletons (S1–S5)

ID	Depth (S2&NWI channels)	ID	Depth	ID	Depth (GE channels)	ID	Depth (channel centerline skeleton)
M01	Initial depth (D)	M08	D + 5m	G1	D + 0.5m	S1	D + 0.5m
M02	D + 0.5m	M09	D + 6m	G2	D + 1m	S2	D + 1m
M03	D + 1m	M10	D + 7m	G3	D + 1.5m	S3	D + 1.5m
M04	D + 1.5m	M11	D + 8m	G4	D + 2m	S4	D + 2m
M05	D + 2m	M12	D + 9m	G5	D + 3m	S5	D + 3m
M06	D + 3m	M13	D + 10m				
M07	D + 4m						

Table 2

Model Scenarios With a Modification of Channels Width for the Network Derived From Sentinel-2 Imagery & National Wetland Inventory (S2&NWI) Before the Modification in Channel Depth (C1, C2, and C3) and After the Modification in Channel Depth (C4, C5, and C6)

ID	Depth (S2&NWI channels)	Channel width
M01	Initial depth (D)	Initial width (W)
C1	D	W + 20m
C2	D	W + 40m
C3	D	W + 60m
M05	D + 2m	W
C4	D + 2m	W + 20m
C5	D + 2m	W + 40m
C6	D + 2m	W + 60m

also updated accordingly. These scenarios are designed to test the sensitivity of tidal propagation to channels width, and to evaluate the effect of a coupled modification in channel width and depth.

5.3. Channel Network Simplification With a Width Threshold

To minimize the increase of tidal prism after modifying channel geometry while keeping the hydro-dynamically important channels unmodified, only channels with a width less than four grid cells (40 m) are dilated to four grid cells (e.g., red color in Figure 9a). The value of four grid cells is determined as optimal in the result section below. Two new model scenarios (U1 and U2) are designed by dilating S2&NWI and the GE network (Figure 9). In these scenarios, the new channel pixels are deepened by 2 m and the bed roughness is updated.

6. Cost Function and Hydrological Connectivity

The bathymetric corrections proposed above provide a method for addressing channel discontinuities. However, they require expensive model trial-and-error, and it is unclear which modifications will lead to improved model performance, or why. It would therefore be ideal to have a fast and simplified method that can achieve similar results without several expensive simulations.

Toward this aim, we have developed a general method for approximating tidal propagation by incorporating both the bathymetry and remotely sensed channel network characteristics into a cost-function surrogate model. This surrogate model approximates the propagation of tides from the coast as a wave front (Sethian, 1996; Sethian & Popovici, 1999) traveling at some “speed” along the channel network, where the speed of propagation is a local function of bed elevation and channel presence. By utilizing this simplified, physically based approach, we are able to simulate the effect that many potential bathymetric modifications will have on improving tidal propagation in the model.

The cost function is designed as follows. First, tidal flow is modeled as a simple linear wave traveling along a least-cost-path from the coastline to everywhere within our domain. To a first order, the speed at which this

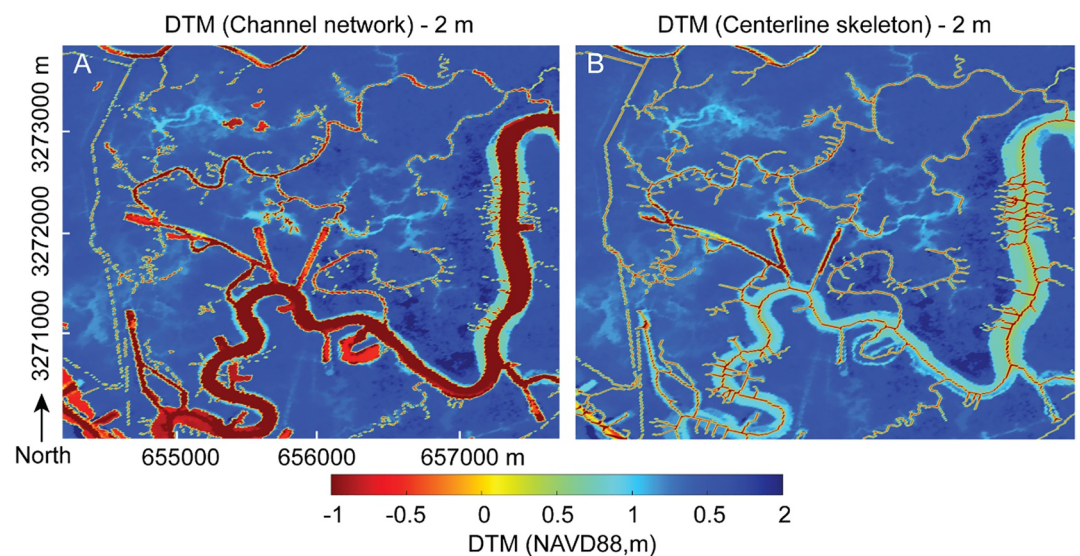


Figure 7. (a) Modified digital terrain model (DTM) based on Sentinel-2 Imagery & National Wetland Inventory network. The channels depth is lowered by 2 m (Figure 3) (b) Modified DTM by lowering depths of channel centerline skeleton. The skeleton is derived from the Google Earth map and has a width of three model grids (Figure 4). This subset is for the visualization purpose (subdomain F in Figure 1).

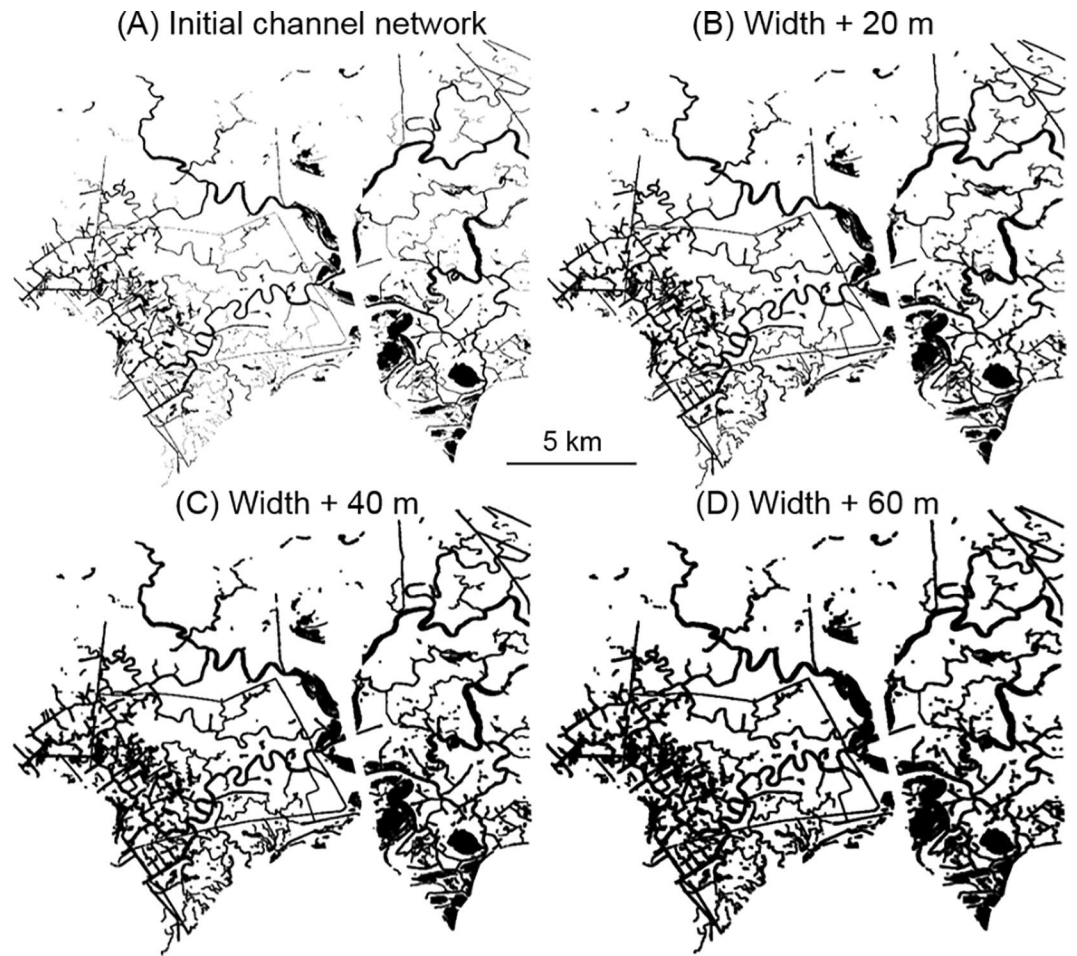


Figure 8. Channel networks with different widths (a) Initial channel networks derived from Sentinel-2 Imagery & National Wetland Inventory. Channels with a width expansion of 1 (b), 2 (c), and 3 cells (d) (20 m, 40 m, and 60 m respectively).

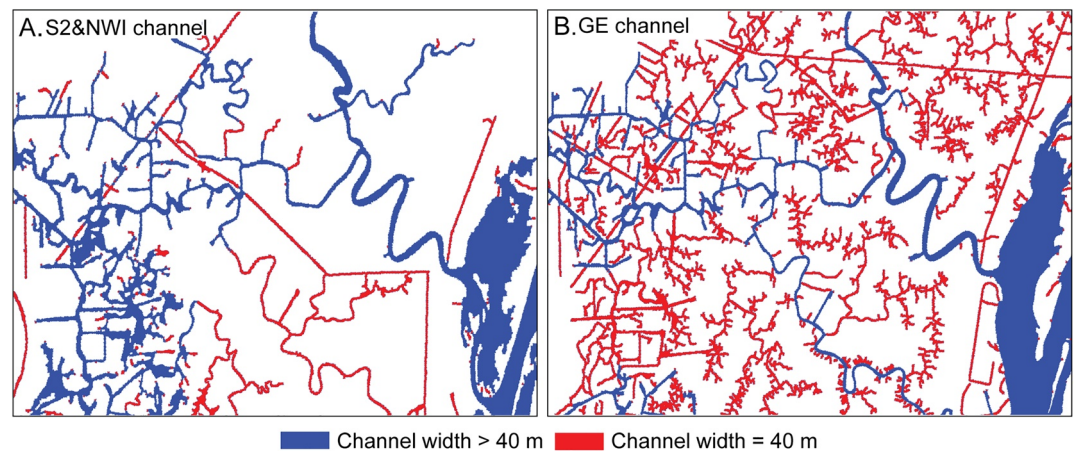


Figure 9. Dilated channel networks with a width threshold of 40 m (the expanded channels with an original width <40 m are shown in red color) (a) Scenario U1 based on Sentinel-2 Imagery & National Wetland Inventory channel network, and (b) scenario U2 based on Google Earth (GE) channel network.

wave should travel in shallow water (if we neglect changes in geometry, friction, etc.) is given by the local celerity in each cell, $C = \sqrt{gd}$, where d is the local flow depth and g is gravity (Lagrange, 1811). To convert from bathymetric elevation to an approximate depth, we assume a water surface elevation equal to mean-high-water (MHW = 0.3 m, NAVD88) in the Wax Lake Delta (Bevington, 2016). Because the bathymetry is known to have errors, in regions where the bed elevation exceeds the water surface elevation, we assign a small (but nonzero) minimum celerity value of 1 m/s. Note that even in shoaling channels bottom elevations above MHW are very unrealistic. This allows for tidal propagation to reach regions which may be hydrologically disconnected, but incentivizes the wave front to first travel through accessible regions. Finally, we model the propagation of the wave front by utilizing the fast-marching algorithm (Sethian, 1996; Sethian & Popovici, 1999) implemented in the open-source Python package scikit-fmm (Furtney, 2019), which assigns each cell in the domain a “first arrival time” for tidal propagation, $\hat{t}_{x,y}$.

It is worth noting that $\hat{t}_{x,y}$ values are not meant to be physically accurate—without accounting for other variables relevant to tidal propagation, such as changes in channel geometry or friction, these travel times are likely to underestimate the true arrival times for tides in the system. Rather, these values are meant to provide a quantifiable benchmark against which to measure how bathymetric changes can improve tidal propagation. When the channels are poorly represented in the bathymetry, regions of abnormally high bed elevation will obstruct tidal propagation, leading to regionally high values of $\hat{t}_{x,y}$. Likewise, when the channels are carved deeper according to some remotely sensed channel network, $\hat{t}_{x,y}$ values will decrease due to cumulative increases in celerity along the least-cost path. This cost-function approach has the advantage of collapsing changes to the channel network mask and changes to the bathymetry into a single measure of performance.

Once this operation has been applied globally to the full unmodified model domain, we take the sum of the $\hat{t}_{x,y}$ values at each of the in-situ gauge sites to obtain S_i , which is a global estimate of the tidal conductivity of the unmodified domain. We then repeat these steps for every proposed bathymetric modification: utilizing some network N and carving depth Δz , the bathymetry is modified, $\hat{t}_{x,y}$ values are re-computed in the modified domain, and we sum along the gauges to obtain $S_i^{N,\Delta z}$, which we normalize by the value S_i for the unmodified domain. After normalizing, any values $S_i^{N,\Delta z}$ which fall below unity represent a modeling scenario in which tidal propagation has been improved. Lastly, for each carving scenario, the volume removed from the system $V^{N,\Delta z}$ is also computed.

This surrogate modeling method allows us to reduce the dimensionality of the problem into a simple optimization problem with two objectives: (a) improve the propagation of tides to each of the in-situ gauges (i.e., minimize $S_i^{N,\Delta z}$), and (b) minimize the amount of modifications made to the bathymetry (i.e., minimize $V^{N,\Delta z}$).

For each channel network, a range of channel depth modifications are tested using the cost-function approach. We test a number of carving depths in the range of $\Delta z \in [0, -10]$ for all channels which fall within a mask delineating the upstream wetlands. We also investigate the importance of different elevation thresholds by testing three cutoff values (−1, −2, and −5), for which a channel is excluded from carving if the thalweg elevation falls below the threshold.

7. Results

7.1. Influence of Channel Deepening on Network Connectivity

At the WL gauges along the WLO, the model performs very well with ME > 0.95 and RMSE < 3 cm. High values of ME are not surprising, because the relatively large water depths (> 15 m) and widths (~300 m) of the WLO allow the correct propagation of the tide. The WLO water elevations thus provide reliable boundary conditions for the flow in secondary channels departing from the WLO and dissecting the wetlands. Modification of channel depths within the wetlands has little influence on water levels along the WLO (Figure 10).

As expected, an increase in distributary channel depth greatly improves model performance (Figures 11a and 11b), especially at the CRMS sites located in shallow channels (e.g., 0482, 4016, 0465, and 6042). The ME of CRMS site 6008 (see the location in Figure 1c) is an exception, since it shows little variations with channel depth. The possible reasons for this discrepancy are: (a) channel connectivity at the site 6008 is controlled by channel width rather than depth, and (b) hydrodynamic blocking may occur along the channels between the WLO and the site.

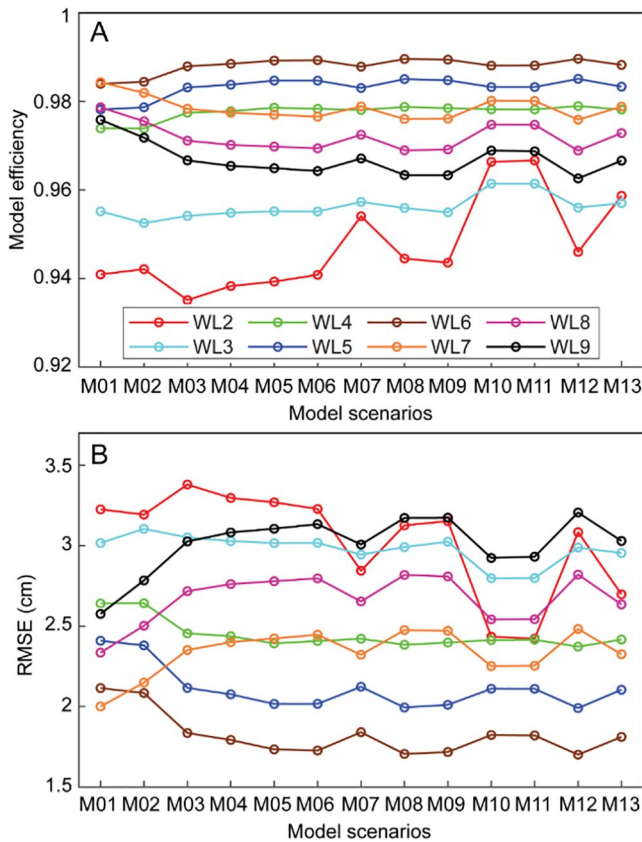


Figure 10. (a) Model efficiency and (b) root mean square error at gauges WL2–WL9 along the Wax Lake Outlet for the 13 model scenarios M01–M13 (Table 1), with increasing modified depths of channels derived from Sentinel-2 Imagery & National Wetland Inventory (Figure 6b).

Channel deepening inevitably enlarges the tidal prism over the wetlands (Figure 11c). Interestingly, the tidal prism increases fast with limited deepening (scenarios M01, M02), and tends to be stable for large increments in water depths (scenarios M05–M13). This is because a moderate deepening would connect shallow channels likely blocked by bathymetric errors, so that more tidal flows can discharge into the wetlands. Once these channels are fully connected, the influence of variations in channel depth on the tidal prism is reduced.

7.2. Influence of Channel Width Expansion on Network Connectivity

The channel width expansion of the original DTM does not increase model efficiency. On the contrary, channel width expansion of the modified DTM of scenario M05 significantly improves model performance, especially at the sites 6008, 0482, and 4016 (Figure 12). This suggests that channel expansion should follow channel deepening, and both adjustments should be implemented to improve channel connectivity in the model. For instance, at site 6008, the channel connectivity is controlled by channel width, while at sites 0482 and 4016 is controlled by both width and depth. The channel deepening based on a channel centerline skeleton with a 3-grid width also shows the importance of channel widths in flow connectivity (Table 3). The skeleton can only guarantee the geometric connectivity of the channel thalwegs, but the unrealistic shallow bathymetry around the thalwegs may prevent tidal propagation (Figure 7b). Therefore, the scenarios based on channel skeletons show little improvement in model performance (Table 3).

7.3. Optimal Channel Depth and Width for Tidal Propagation

Since the real bathymetry within the channels and the tidal prism over the system is unknown, in practice the optimal modification scenario should provide the best model performance (calibrated by tidal gauges) with least modification of tidal prism. An alternative way to preserve the tidal prism

is to remove the hydrodynamically unimportant small-scale channels and expand channels with a width below a threshold (Figure 9). Results show that the dilated S2&NWI channel network with a 2 m depth threshold and a 40 m width threshold (4 mesh elements) performs best, with the average model efficiency of 0.71, RMSE of 7.72 cm, and an increase in tidal prism of 55% (Tables 4 and 5).

7.4. Validation With Discharge Data Collected in 2021

All scenarios of bathymetric modifications are then implemented with 2021 flow boundary conditions, and the modeled discharges are compared to field measurements at five cross sections (Figures 1g and 1h). Generally, the M01 scenario using the initial bathymetry underestimates the cross-sectional discharge. While both channel deepening and width expansion lead to an increase of discharge, the width expansion works only after channel deepening (Figure 13). For instance, the discharge at CS-1 increases from 14.8 m³/s (scenario C1) to 22.0 m³/s (scenario C3), while after channel deepening, the discharge increases from 68.3 m³/s (scenario C4) to 108.8 m³/s (scenario C6), corroborating the importance of channel depths on channel hydrological connectivity.

Since the discharges at CS-3 and CS-4 are very small, only the discharges CS-1, CS-2, and CS-5 are used for error evaluation (Table 6). The error reduces from 30.9% (M01) to 12.9% (M05) and 19.9% (U1), respectively. A general trend in discharge is noticeable when the channels are deepened or enlarged (Figure 13). Discharge is underestimated with the original topography because the poor channel connectivity hinders tidal propagation. When channels are deepened and enlarged, the discharge increases to values close to the measured ones, indicating more realistic tidal propagation. However, the tidal prism is overestimated when widths and depths are too large, leading to discharges much higher than the measured ones (Figure 13).

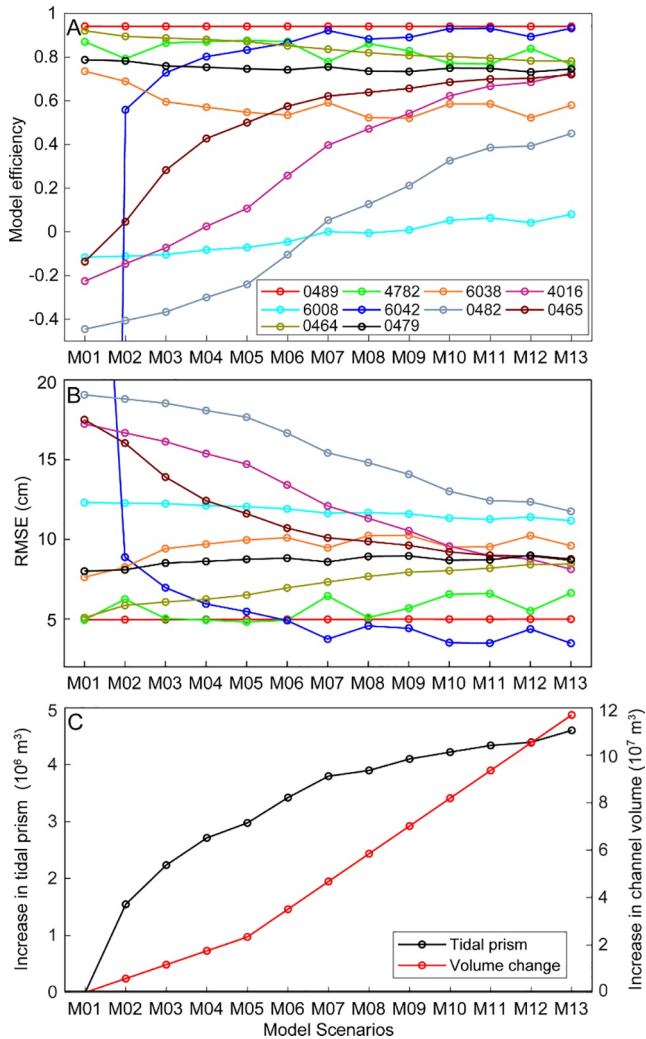


Figure 11. (a) Model efficiency and (b) root mean square error at 10 Coastwide Reference Monitoring System sites for 13 model scenarios M01–M13 obtained by increasing the depth of channels derived from Sentinel-2 Imagery & National Wetland Inventory (Figure 6B). (c) Changes in tidal prism and channel volume within the western wetlands for the 13 model scenarios M01–M13 (Table 1).

7.5. Comparison With Surrogate Model

We find that the surrogate model based on the cost function successfully captures, at least qualitatively, much of the behavior observed in the full-scale hydrodynamic model. Compared to the base case (Figure 14a), we observe considerable improvement in values of $\hat{t}_{x,y}$ in many regions of the wetlands upstream of the WLD after modifying the bathymetry (e.g., Figures 14b and 14c). The locations of change are strongly dependent on underlying differences in the network used, as can be seen from comparing the maps obtained with the S2&NWI network (Figure 14b) and the Google Earth network (Figure 14c) for the same carving depth and elevation threshold. Similarly, the method seems very sensitive to the locations and scale of the errors in the bathymetry, as the most apparent differences in $\hat{t}_{x,y}$ occur once the extent of modification is large enough to “re-activate” (i.e., hydrologically reconnect) channels to the main distributary network. We see comparatively little change in $\hat{t}_{x,y}$ values along the Wax Lake Outlet, meaning that channel modifications in the wetlands minimally influence water levels in the main channel.

When comparing the improvement in tidal travel times $S_t^{N,\Delta z}$ to the volume removed from the system $V^{N,\Delta z}$, we observe a classic pareto-front behavior (Figure 15), wherein improving the performance toward one objective function tends to decrease the performance toward the other. Starting from the base case with no modifications to the bathymetry (S_t , the intercept for each curve in Figure 15), as we increase the carving depth Δz (values shown inside each marker), the more improvement we see in the reduction of $S_t^{N,\Delta z}$. Each curve represents a different network used (Google Earth or S2&NWI) and elevation threshold for carving (–1, –2, and –5). At first, the improvement in $S_t^{N,\Delta z}$ is rapid for very small changes in $V^{N,\Delta z}$, indicating the re-activation of many channels which had previously been disconnected from the main distributary network. This finding is similar to the results of numerical modeling. However, as Δz continues to increase, after some threshold we begin to see diminishing returns, at which point $V^{N,\Delta z}$ is increasing at a rate much greater than $S_t^{N,\Delta z}$ is decreasing. After very unrealistic amounts of carving (e.g., 5 m), each of these curves stabilizes to approximately the same constant slope, indicating that no additional blockages are being removed by additional carving.

In this analysis, we choose the inflection point of each curve as representing the optimal carving depth for that choice of network/elevation threshold (inflection points for each curve are highlighted in the inset of Figure 15).

We compute the inflection point as the smallest carving depth at which the slope of the curve stabilizes to near the mean value we observe at unrealistically large carving depths, for which we select a (conservative) slope threshold of -1.2 km^{-3} for this application. We consider this point to be the optimal balance between each competing objective because it indicates that all the blockages contained within the channel network have been removed, which is exactly what we observe in our full-scale modeling simulations. Of the networks tested, we find that the S2&NWI network consistently performs better than the Google Earth network for the same volume carved. We also find that the choice of elevation threshold can have a small but visible impact on the shape of each curve, with the least restrictive threshold (–5 m) performing the best for each network. Higher additional threshold elevations were tested, but are not shown as they are found to minimally differ beyond –5 m. Interestingly, the choice of network and threshold seems to minimally impact the location of the inflection point, which sits around $\Delta z \approx 2\text{--}3$ m for all scenarios (inset of Figure 15).

The surrogate modeling results align with our hydrodynamic model results, in which the S2&NWI network carved to a minimum depth of 2 m performed optimally for improving the tidal signal at the reference gauges without dramatically increasing the volume removed from the system (Table 5). This suggests that the scale

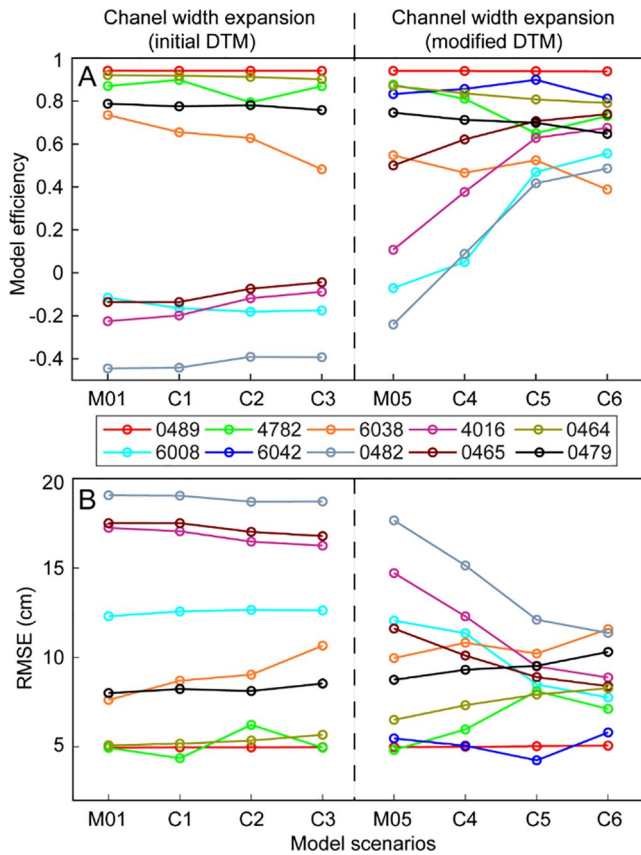


Figure 12. Model results with channel width expansion before (left) and after a modification in channel depth (right) (a) Model efficiency and (b) root mean square error at 10 Coastwide Reference Monitoring System (CRMS) sites for channel expansion scenarios C1–C3 based on the initial digital terrain model (DTM) (M01) and C4–C6 based on the modified DTM M05 (Tables 1 and 2). The values of CRMS-6042 are out of the axis limits in left panels. The elevation in the expanded channels is calculated by averaging values of adjacent channel pixels.

of bathymetric errors important to tidal propagation in the model is around 2–3 m.

Unfortunately, the surrogate model is insensitive to changes in channels width. Despite this, determining the optimum channel depth as a first step based on the surrogate model will substantially reduce the need for expensive Delft3D simulations. The relevant code is provided in the link <https://deltax.jpl.nasa.gov/data/MRD/preliminary/2021-12-delft3D-model/>.

8. Discussion

Modeling hydrodynamics within coastal wetlands dissected by complex channel networks is challenging due to inevitable bathymetric errors. These errors preclude the appropriate representation of channels in the model and prevent realistic tidal propagation. Without a correct flow propagation along the channels, the calculation of water fluxes is unreliable. Model accuracy is therefore related to the design of the numerical grid and data fusion into the grid.

8.1. Bathymetric Errors and Channel Network Extraction

Upscaling fine-resolution topography data (e.g., 1 m LIDAR) to coarse-grid models by smoothing (arithmetic mean of the data) often leads to inappropriate representations of hydrodynamic blocking features. Examples are the loss of levee heights and narrow channels in coastal hydrodynamic models (Hodges, 2015; Li & Hodges, 2019) and wall height in flood inundation models (Yu & Lane, 2011). The 10 m DTM used herein was also smoothed (Figure 6a). The smoothing may have caused unrealistic shallow bathymetry in channels, leading to errors in tidal propagation. Because of these bathymetric problems, most modeling work in the WLD has focused on the delta itself (Edmonds & Slingerland, 2010; Liu et al., 2018; Olliver et al., 2020), without considering the influence of the large-scale adjacent wetlands on hydrodynamics and sediment transport.

Large efforts have been made to automatically extract channel networks from either the DTM or imagery. The early study of Fagherazzi et al. (1999) used a

Table 3
Model Efficiency and Root Mean Square Error (RMSE) for Model Scenarios S1–S5 (Tables 1) in 10 Coastwide Reference Monitoring System (CRMS) Field Sites

CRMS ID	Model efficiency (ME)					RMSE (cm)				
	S1	S2	S3	S4	S5	S1	S2	S3	S4	S5
S0489	0.94	0.94	0.94	0.94	0.94	4.94	4.95	4.96	4.96	4.96
S6008	−0.06	−0.07	−0.06	−0.04	−0.02	11.97	12.05	11.96	11.85	11.74
S4782	0.86	0.88	0.91	0.83	0.89	5.06	4.76	4.15	5.73	4.50
S6042	0.62	0.80	0.84	0.87	0.85	8.23	5.97	5.29	4.81	5.18
S6038	0.84	0.81	0.79	0.79	0.75	5.96	6.43	6.72	6.71	7.42
S0482	−0.44	−0.45	−0.40	−0.35	−0.29	19.01	19.09	18.79	18.41	17.99
S4016	−0.22	−0.22	−0.18	−0.13	−0.08	17.19	17.20	16.89	16.56	16.15
S0465	0.14	0.26	0.37	0.45	0.53	15.23	14.16	13.07	12.22	11.31
S0464	0.93	0.93	0.92	0.92	0.91	4.90	4.93	4.99	5.10	5.39
S0479	0.79	0.78	0.78	0.78	0.77	7.95	8.10	8.13	8.07	8.31

Table 4
Model Efficiency and Root Mean Square Error (RMSE) for Model Scenarios M01, M05, C5, G4, U1, and U2 (Tables 1 and 2) at 10 Coastwide Reference Monitoring System (CRMS) Field Sites

CRMS ID	Model efficiency (ME)						RMSE (cm)					
	M01	M05	C5	G4	U1	U2	M01	M05	C5	G4	U1	U2
S0489	0.94	0.94	0.94	0.94	0.94	0.94	4.94	4.98	5.03	4.98	5.00	5.00
S6008	-0.13	-0.07	0.47	0.12	0.41	0.13	12.39	12.05	8.48	10.91	8.91	10.84
S4782	0.89	0.88	0.65	0.87	0.87	0.83	4.61	4.82	8.11	4.86	5.01	5.66
S6042	-13.12	0.83	0.90	0.88	0.90	0.80	50.24	5.47	4.24	4.72	4.18	6.01
S6038	0.85	0.55	0.52	0.80	0.81	0.69	5.79	9.96	10.21	6.55	6.49	8.23
S0482	-0.49	-0.24	0.42	-0.03	0.28	0.02	19.38	17.66	12.11	16.10	13.46	15.73
S4016	-0.25	0.11	0.63	0.46	0.51	0.55	17.38	14.72	9.49	11.43	10.87	10.48
S0465	0.17	0.50	0.71	0.64	0.73	0.68	14.98	11.61	8.89	9.86	8.57	9.32
S0464	0.92	0.87	0.81	0.86	0.87	0.82	5.01	6.50	7.92	6.67	6.47	7.72
S0479	0.79	0.75	0.70	0.75	0.77	0.73	7.87	8.74	9.52	8.66	8.25	9.03
Average	-0.94	0.51	0.67	0.63	0.71	0.62	14.26	9.65	8.40	8.47	7.72	8.80

combination of threshold elevation and threshold curvature from DTM to obtain an accurate channel network in the Venice Lagoon, Italy. 80% of the extracted network well matched high-resolution satellite imagery. Recently, the development of sophisticated algorithms like the geodesic approach (Passalacqua et al., 2010), the lowest path identification with a characteristic sediment volume (Hiatt et al., 2020; Kleinhans et al., 2019), and a model based on flow path tracking method (Limaye, 2017) have significantly increased the accuracy of channel network extraction. However, these topography-based methods ignore the accuracy of the topographic data, potentially leading to errors in channel network extraction. For example, the WLD analyzed in this study is a low-lying delta with a micro tide, so that the elevation threshold between water and land, as well as the inundation extent are very sensitive to topographic errors (Alizad et al., 2020). Instead, network identification from aerial images using spectral thresholds or classification algorithms is more accurate, but may require manual intervention to maintain channel connectivity because of uncertainty in the classification of mixed features (Isikdogan et al., 2015; Jin et al., 2021; Passalacqua et al., 2013).

8.2. Model Grid Obtained With Fusion of Remote Sensing Data

Both structured and unstructured grids are commonly used in coastal hydrodynamic models (Donatelli et al., 2020). Compared to structured grids, unstructured grids (e.g., triangular) are more flexible and can be locally refined and reshaped to match edges of small-scale channels. These grids can maximize the resolution of topographic features (Bates et al., 2003), but are prone to errors in data projection and fusion with remote sensing data. This is because remote sensing imagery is typically organized on Cartesian grids that do not match the spatial varying size and shape of an unstructured grid. For example, the use in this study of a ~10 m quasi-Cartesian curvilinear grid has largely reduced errors in the assignment of bed roughness values from a 10 m Sentinel-2 classification map.

Numerical models using same resolution of remote sensing grids would reduce upscaling uncertainties, but it might become too computationally demanding. Therefore, modelers must evaluate the trade-offs between spatial resolution, uncertainties in data projection and data fusion, and computation resources. In our case, we chose to increase the model spatial resolution (~10 m) to reduce the uncertainty in data projection, and considered acceptable a computational time of 10 hr to simulate 30 days of hydrodynamics on a supercomputer cluster (2 nodes × 28 cores).

Table 5
Comparison of Different Model Scenarios

Case ID	Base network	Width (m)	Depth (m)	Tidal prism (normalized)
M01	/	/	/	1
M05	S2&NWI	/	+2 m	1.48
C5	S2&NWI	+40m	+2 m	2.93
G4	Google Earth	/	+2 m	1.67
U1	S2&NWI	40 m	+2 m	1.55
U2	Google Earth	40 m	+2 m	1.95

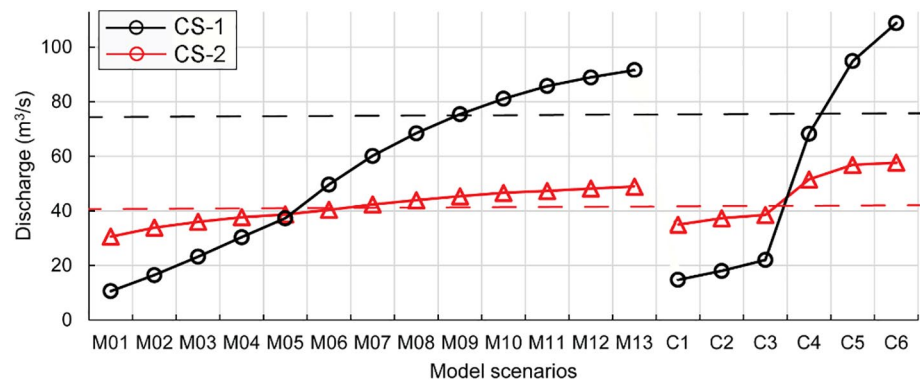


Figure 13. Modeled discharges at cross sections CS-1 and CS-2 for the 13 model scenarios M01–M13 (Table 1) and C1–C5 (Table 2). Dash lines indicate field measurements of discharge at cross sections CS-1 (black) and CS-2 (red).

8.3. Model Calibration and Validation

Coastal models are generally calibrated with few tidal or velocity gauges because of the high cost of field observations (Zhang et al., 2020). In our study domain, 18 water level stations cover not only the main channel (WLO), but also the complex creeks network, well capturing the delay in tidal propagation and the flow attenuation over the entire system. The discharge at five cross sections was also evaluated, demonstrating the necessity of channel deepening to promote channel hydrological connections. Based on errors between modeled and measured discharges, the optimal channel geometry is scenario M05, followed by scenario U1 which is the one producing the smallest discharge error. The small discrepancy between discharge and water level calibrations may be caused by the limited number of discharge observations, therefore we stress the importance of comprehensive discharge data for model calibration (Hanegan, 2011). Future modeling work should also use field data to calibrate velocities in shallow tidal channels. In fact, it was found that subtle topography variations dominate flow velocities and flow reversals in tidal flats and salt marshes (Torres & Styles, 2007). Flow velocities are also very sensitive to the accuracy of bottom bathymetry in hydrodynamic models (Wang et al., 2009).

Our results highlight the importance of spatially dense observations for model calibration. One could always obtain a satisfying model performance ($ME > 0.95$) using only the eight gauges along the main channel (WLO), but gauges within the marsh are needed to determine whether wetland channels are blocked (see the M01 scenario). Similarly, Jiang et al. (2019) calibrated a 1-D river hydraulic model of the Songhua River, China, using satellite altimetry, and stressed that a high spatial resolution is more important than high temporal resolution and altimetry accuracy. Remote sensed hydrodynamic observations are expected to significantly improve the performance of coastal models: the upcoming Surface Water and Ocean Topography (SWOT) satellite mission will provide relatively high spatial and temporal observations of water surface elevations (Pitcher et al., 2019);

Table 6
Modeled Discharges at Cross Sections CS-1 to CS-5 for Model Scenarios M01, M05, C5, G4, U1, and U2 (Tables 1 and 2)

Model scenarios	Field discharge	Field sites					ME	RMSE	Error
		CS-1	CS-2	CS-3	CS-4	CS-5			
		74.65	40.01	1.03	1.06	10.11			
	M01	10.62	30.59	0.71	0.10	6.39	-0.04	28.99	30.9%
	M05	37.32	38.72	0.58	0.66	6.38	0.65	16.79	12.9%
	C5	94.89	56.87	0.29	0.82	3.99	0.82	12.10	20.6%
	G4	41.94	45.50	0.43	0.22	3.48	0.72	15.13	21.4%
	U1	47.16	48.86	0.13	0.13	3.61	0.78	13.25	19.9%
	U2	34.82	52.44	0.96	2.24	3.21	0.56	18.92	28.2%

Note. Error between the model (M) and field data (D) is calculated as $\frac{1}{n} \sum_{i=1}^n \frac{M_i - D_i}{D_i}$, where n is number of sites ($n = 3$, for sites CS-1, CS-2, and CS-5).

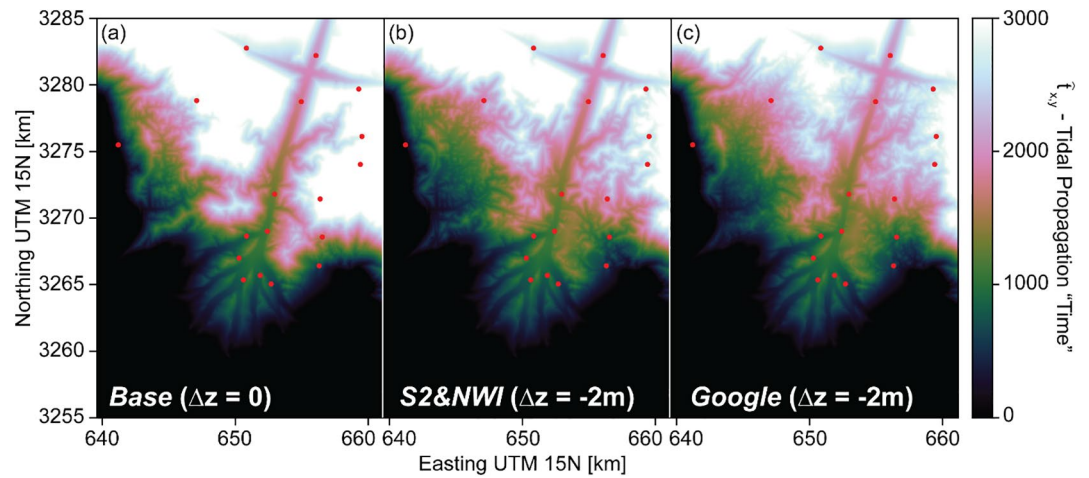


Figure 14. Cost-function maps of $\hat{t}_{x,y}$ (tidal propagation time) for three examples of bathymetry input: (a) the bathymetry or base case, against which all other runs are compared, (b) the Sentinel-2 Imagery & National Wetland Inventory network after applying a carving depth $\Delta z = -2$ m, and (c) the Google network after applying a carving depth $\Delta z = -2$ m (Table 1). The reference in situ gauges are shown in red, along which we sum $\hat{t}_{x,y}$ values to obtain S_t . Times shown in (b) and (c) represent an elevation threshold of -5 m.

Synthetic Aperture Radar (SAR)-derived data will measure 2-D flow inundation (e.g., Ayoub et al., 2018) and water-level change using repeat-pass interferometry (e.g., Liao et al., 2020).

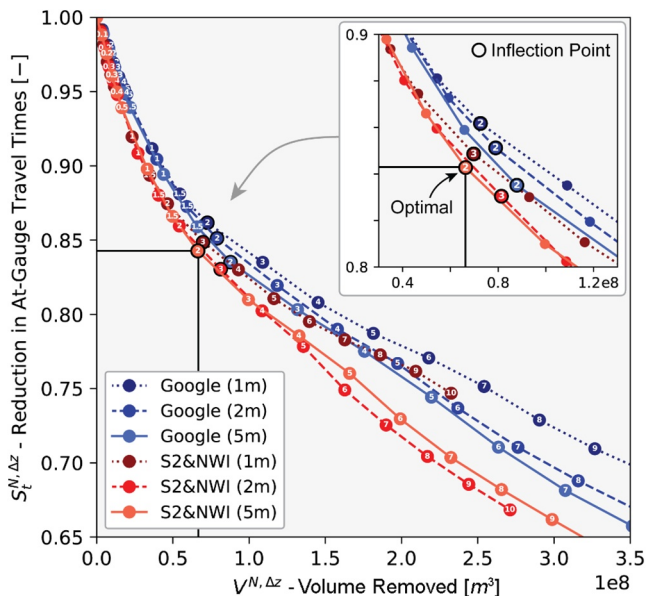


Figure 15. Comparison between the reduction in tidal travel times $S_t^{N,\Delta z}$ and the volume removed from the system $V^{N,\Delta z}$. The carving depth Δz is indicated in white inside each marker. All curves are equal at the intercept which represents the unmodified bathymetry. Lower values of $S_t^{N,\Delta z}$ represent improved tidal propagation. The inflection points, which represent the optimum for each curve, are shown in the zoomed-in inset and outlined in black. The optimal bathymetry correction is indicated and corresponds to the Sentinel-2 Imagery & National Wetland Inventory map shown in Figure 13b.

In coastal models, errors can arise because of the poor representation of the geometry (i.e., bathymetry), lack of data at the boundaries (i.e., boundary conditions), or because of poor calibration of model coefficients (e.g., friction coefficients of Cunge, 2003). In our modeling framework the bathymetry is the main source of error, and in particular the representation of tidal channels and small creeks. The model efficiency is in fact very high along the Wax Lake Outlet (gauges WL2–WL9, see Figure 10) with a RMSE less than 4 cm. This indicates that channel friction, riverine and tidal boundary conditions are more than adequate to capture tidal propagation along the main river. On the contrary, the model efficiency is very uneven for the creeks in the marsh interior. At some of the creek gauges the modeled water oscillations are strongly damped (RMSE of 20 cm with a tidal range of 36 cm) so that any possible change of friction coefficient would not address the problem. Moreover, a selective adjustment of the friction coefficient in some creeks but not in others would not be realistic. Our simulations clearly indicate that water is unable to flow in some channels because of bathymetric errors in the modeling mesh. We therefore conclude that in coastal wetlands the poor representation of tidal channels is among the main sources of error. This is because the channel network is bathymetrically very complex, with very sharp bottom gradients within few meters (some of the channel banks are almost vertical).

8.4. Utilization of the Simplified Cost Function to Assess Network Connectivity

In coastal wetlands, the bathymetry of tidal channels is very often unknown or subject to large errors. Remote sensors cannot detect channels bottomsets and bathymetric surveys are often limited to the main navigable waterways. There is therefore a need to refine channel bathymetry with physically based, automated algorithms.

Despite its simplicity, our cost function method appears capable of estimating the optimal bathymetric corrections for improving tidal propagation in a full-scale hydrodynamic model. This method is computationally efficient and only relies on knowledge of bathymetry and network. It can be used to quickly compare hundreds of potential bathymetric corrections without running the full Delft3D model. Further, because this method is not domain or grid-size dependent, it can be potentially used to improve any coastal model attempting to accurately reflect tidal processes with unreliable bathymetric data.

While the surrogate model is able to accurately predict optimal changes in depth to capture tidal propagation, it is unable to detect how changes in width will affect model performance. The geodesic approach utilized by the fast-marching algorithm is not sensitive to the thickness of the least-cost-path from the coast, and as such does not reflect the importance of channel geometry to tidal propagation in the model. It is possible that a similar cost function could be devised to account for the role of width in tidal propagation, but we hypothesize that doing so will be nontrivial for a few reasons. Both shallow depths and narrow widths can obstruct tidal propagation—however, the former is related to simple errors in input data, whereas the latter is a complex function of channel form drag in the model due to factors like grid size, channel direction, and sinuosity. Because the cost-function approach does not rely on any information about the model itself, it is hard to know a priori what effect channel width will have on tidal propagation.

From our modeling results, it is clear that artificially dilating channel widths to a minimum of four cells (40 m) can improve model performance, on top of the aforementioned depth modification. We hypothesize that the scale at which wetland channels are able to accurately represent tidal processes is on the order of $\approx 4\Delta x$, above which performance tends to plateau (e.g., as is the case with the wide Wax Lake Outlet, which performs well across all scenarios tested here). We recommend utilizing our simple surrogate model to determine the optimal depth correction to improve tidal propagation, after which model trial-and-error can be minimized to investigating the importance of channel width. In this way, the simple method proposed here can help narrow the required number of full-scale model simulations considerably.

8.5. Is the Small Structure of the Channel Network Important?

The results of our simulations indicate that the representation of the small structure of the network (channels with width smaller than 10 m) does not improve model results. Simulations with the Google Earth channel network, which represents all channels visible from a high resolution aerial image (see Figure 9b), yield an average ME of 0.63 and a RMSE of 8.47 cm in terms of water levels (scenario G4 Table 4), which are slightly better than the simulation with the network obtained from the Sentinel-2 image S2&NWI (scenario M05, ME = 0.51, RMSE 9.65 cm). This is because with more channels tidal propagation is faster, therefore counteracting the blocking effect of the bathymetric errors. However, the average discharge error with the Google Earth network is 21.4% (Table 6), much higher than the error with the S2&NWI network (12.9%). In fact the representation of small channels requires the incision of many mesh elements, increasing the tidal prism (Table 5). If the width of the channel network is expanded by two elements, the model with the S2&NWI network is actually superior in terms of water levels (scenario U1 ME = 0.71 RMSE = 7.72 cm vs. scenario U2 ME = 0.62 RMSE = 8.80 cm), and the average discharge error of the Google Earth network is much higher (28.2% for U2 vs. 19.9% for U1). We therefore conclude that overall the inclusion of small channels detected at a resolution below the model mesh might be not worthy, since improves little water levels but leads to errors in discharge. The utilization of a network extracted from a remote sensing image with the same resolution of the model mesh (10 m) seems optimal for tidal propagation within the channels.

8.6. Application to Other Coastal Systems

Our results can be generalized to all shallow coastal environments dissected by channels, including salt marshes, mangroves, deltaic wetlands, and tidal flats. Tidal propagation in the channel network must be correctly simulated to capture fluxes of water, sediments, and nutrients (e.g., Fagherazzi et al., 2013). When using a Cartesian mesh, modification to the channel bathymetry is required to eliminate possible obstacles to flow propagation. The following steps should be taken to correctly represent channel hydrodynamics: (a) a high-quality channel network should be derived from satellite images at a resolution identical to the computational grid; all the channels should be connected (see Jin et al., 2021 for an example of channel extraction); (b) bottom friction and

boundary conditions should be calibrated in the largest channels, where the tidal and river flow can propagate unobstructed; (c) a minimum water depth derived from our cost function should be prescribed in the channels; (d) the width of the small channels should be increased to a minimum of four grid elements. Our approach can be easily automated, enabling the representation of channel networks in large coastal domains.

9. Conclusions

It is challenging to model tidal propagation along complex channel networks that flood and drain coastal wetlands, because bathymetric errors lead to an underestimation of channel geometric connectivity (e.g., blocking effects). Based on a unique richly gauged coastal wetland (18 water-level gauges covering the entire system), we build a ~10 m hydrodynamic model from a 10 m topography data set, and evaluate the influence of channel geometry (width and depth) on channel connectivity and model performance. A series of channel networks derived from remote sensing imagery are tested to constrain channel width and depth and achieve the optimal channel network for tidal propagation. We provide a general framework to improve model performance by integrating high-resolution imagery and bathymetry, without a significant increase in tidal prism. The main conclusions of the study are:

1. Subtle bathymetric variations dominate the accuracy of hydrodynamic modeling in shallow wetland channels, but have little effect on deep channels (for example, along the Wax Lake Outlet). This result stresses the need of spatially dense observations for model calibration.
2. Several factors contribute to blocking tidal propagation in wetland channels. Among them, we focus here on errors in channel depth due to topographic smoothing and low grid resolution in narrow channels. A minimum 2 m channel depth and four grid elements channel width (40 m) are required to capture flow propagations in our ~10 m resolution model.
3. Increasing channel depth can enhance channel connectivity, but can also lead to an overestimation of tidal prism and therefore discharge in the wetlands. The tidal prism substantially increases even with a small increase in channel depth.
4. An increase of 2 m for the water depth of the channels produce optimal results for our hydrodynamic model of WLD. This conclusion is verified by a simplified cost function method for estimating corrections to the structural connectivity of the channel network, which can be applied to other coastal wetlands.
5. The inclusion of small channels with a width smaller than the mesh resolution does not increase the performance of the model with respect to water levels and discharge.
6. The combination of numerical simulations and a simplified cost function, as well as channel networks derived from remote sensing, can efficiently determine the optimal water depth and width of channels for modeling the propagation of tidal and riverine signals.

Conflict of Interest

The authors declare no conflicts of interest relevant to this study.

Data Availability Statement

The simulations data and codes of cost-function surrogate model are available at <https://deltax.jpl.nasa.gov/data/MRD/final/2022-02-delft3D-model/>.

References

- Alizad, K., Medeiros, S. C., Foster-Martinez, M. R., & Hagen, S. C. (2020). Model sensitivity to topographic uncertainty in meso- and microtidal marshes. *IEEE Journal of Selected Topics in Applied Earth Observations and Remote Sensing*, *13*, 807–814. <https://doi.org/10.1109/JSTARS.2020.2973490>
- Allen, J. L., Somerfield, P. J., & Gilbert, F. J. (2007). Quantifying uncertainty in high-resolution coupled hydrodynamic-ecosystem models. *Journal of Marine Systems*, *64*(1–4), 3–14. <https://doi.org/10.1016/j.jmarsys.2006.02.010>
- Ayoub, F., Jones, C. E., Lamb, M. P., Holt, B., Shaw, J. B., Mohrig, D., & Wagner, W. (2018). Inferring surface currents within submerged, vegetated deltaic islands and wetlands from multi-pass airborne SAR. *Remote Sensing of Environment*, *212*(April), 148–160. <https://doi.org/10.1016/j.rse.2018.04.035>
- Bates, P., Marks, K., & Horritt, M. (2003). Optimal use of high-resolution topographic data in flood inundation models. *Hydrological Processes*, *17*(3), 537–557. <https://doi.org/10.1002/hyp.1113>
- Bevington, A. E. (2016). *Dynamics of land building and ecological succession in a prograding deltaic floodplain, Wax Lake delta, LA, USA*.

Acknowledgments

The NASA Delta-X project is funded by the Science Mission Directorate's Earth Science Division through the Earth Venture Suborbital-3 Program NNH17ZDA001N-EVS3. This work was partly conducted by the Jet Propulsion Laboratory, California Institute of Technology, under contract with the National Aeronautics and Space Administration. Sergio Fagherazzi was also partially funded by NSF grants DEB-1832221 to the Virginia Coast Reserve Long-Term Ecological Research project and OCE-1637630 to the Plum Island Ecosystems Long-Term Ecological Research project.

- Carle, M. V., Sasser, C. E., & Roberts, H. H. (2015). Accretion and vegetation community change in the Wax Lake Delta following the historic 2011 Mississippi River flood. *Journal of Coastal Research*, 31(3), 569–587. <https://doi.org/10.2112/JCOASTRES-D-13-00109.1>
- Cea, L., & French, J. R. (2012). Bathymetric error estimation for the calibration and validation of estuarine hydrodynamic models. *Estuarine, Coastal and Shelf Science*, 100, 124–132. <https://doi.org/10.1016/j.ecss.2012.01.004>
- Center for Operational Oceanographic Products and Services (Co-Ops) (2018). *CO-OPS water level data from the coastal tide gauge and great lake water level network of the United States and US territories*. NOAA National Centers for Environmental Information. <https://doi.org/10.25921/dt9g-2p60>
- Chow, V. T. (1959). *Open channel flow*. McGraw-Hill Book Company.
- Christensen, A., Twilley, R. R., Willson, C. S., & Castañeda-Moya, E. (2020). Simulating hydrological connectivity and water age within a coastal deltaic floodplain of the Mississippi River Delta. *Estuarine, Coastal and Shelf Science*, 245, 106995. <https://doi.org/10.1016/j.ecss.2020.106995>
- Christensen, A. L., Mallard, J. M., & Nghiem, J. (2021). *Delta-X: Acoustic doppler current profiler channel surveys, coastal Louisiana, 2021*. ORNL DAAC. <https://doi.org/10.3334/ORNLDAAC/1939>
- Chust, G., Grande, M., Galparsoro, I., Uriarte, A., & Borja, Á. (2010). Capabilities of the bathymetric hawk eye LiDAR for coastal habitat mapping: A case study within a Basque estuary. *Estuarine, Coastal and Shelf Science*, 89(3), 200–213. <https://doi.org/10.1016/j.ecss.2010.07.002>
- Cunge, J. A. (2003). Of data and models. *Journal of Hydroinformatics*, 5(2), 75–98. <https://doi.org/10.2166/hydro.2003.0007>
- Defina, A. (2000). Two-dimensional shallow flow equations for partially dry areas. *Water Resources Research*, 36(11), 3251–3264. <https://doi.org/10.1029/2000WR900167>
- Denbina, M. W., Simard, M., Pavelsky, T. M., Christensen, A. I., Liu, K., & Lyon, C. (2020). *Pre-delta-X: Channel bathymetry of the Atchafalaya basin, LA, USA, 2016*. ORNL DAAC. <https://doi.org/10.3334/ORNLDAAC/1807>
- Donatelli, C., Ganju, N. K., Zhang, X., Fagherazzi, S., & Leonardi, N. (2018). Salt marsh loss affects tides and the sediment budget in shallow bays. *Journal of Geophysical Research: Earth Surface*, 123, 2647–2662. <https://doi.org/10.1029/2018JF004617>
- Donatelli, C., Zhang, X., Ganju, N. K., Aretxabaleta, A. L., Fagherazzi, S., & Leonardi, N. (2020). A nonlinear relationship between marsh size and sediment trapping capacity compromises salt marshes' stability. *Geology*, 48(10), 966–970. <https://doi.org/10.1130/G47131.1>
- Edmonds, D., & Slingerland, R. (2010). Significant effect of sediment cohesion on delta morphology. *Nature Geoscience*, 3(2), 105–109. <https://doi.org/10.1038/ngeo730>
- Fagherazzi, S. (2008). Self-organization of tidal deltas. *Proceedings of the National Academy of Sciences*, 105(48), 18692–18695. <https://doi.org/10.1073/pnas.0806668105>
- Fagherazzi, S., Bortoluzzi, A., Dietrich, W. E., Adami, A., Lanzoni, S., Marani, M., & Rinaldo, A. (1999). Tidal networks 1. Automatic network extraction and preliminary scaling features from digital terrain maps. *Water Resources Research*, 35(12), 3891–3904. <https://doi.org/10.1029/1999WR900236>
- Fagherazzi, S., Kirwan, M. L., Mudd, S. M., Guntenspergen, G. R., Temmerman, S., D'Alpaos, A., & Clough, J. (2012). Numerical models of salt marsh evolution: Ecological, geomorphic, and climatic factors. *Reviews of Geophysics*, 50(1), RG1002. <https://doi.org/10.1029/2011RG000359>
- Fagherazzi, S., Mariotti, G., Leonardi, N., Canestrelli, A., Nardin, W., & Kearney, W. S. (2020). Salt Marsh dynamics in a period of accelerated sea level rise. *Journal of Geophysical Research: Earth Surface*, 125(8), e2019JF005200. <https://doi.org/10.1029/2019JF005200>
- Fagherazzi, S., Wiberg, P. L., Temmerman, S., Struyf, E., Zhao, Y., & Raymond, P. A. (2013). Fluxes of water, sediments, and biogeochemical compounds in salt marshes. *Ecological Processes*, 2(1), 1–16. <https://doi.org/10.1186/2192-1709-2-3>
- FitzGerald, D. M., & Hughes, Z. (2019). Marsh processes and their response to climate change and sea level rise. *Annual Review of Earth and Planetary Sciences*, 47(1), 481–517. <https://doi.org/10.1146/annurev-earth-082517-010255>
- Friedrichs, C. T., & Aubrey, D. G. (1988). Non-linear tidal distortion in shallow well-mixed estuaries: A synthesis. *Estuarine, Coastal and Shelf Science*, 27(5), 521–545. [https://doi.org/10.1016/0272-7714\(88\)90082-0](https://doi.org/10.1016/0272-7714(88)90082-0)
- Furtney, J. (2019). scikit-fmm: The fast marching method for Python. accessed on 4 March 2021. Retrieved from <https://github.com/scikit-fmm/>
- Ganju, N. K., Defne, Z., Kirwan, M. L., Fagherazzi, S., D'Alpaos, A., & Carniello, L. (2017). Spatially integrative metrics reveal hidden vulnerability of microtidal salt marshes. *Nature Communications*, 8(1), 14156. <https://doi.org/10.1038/ncomms14156>
- Grill, G., Lehner, B., Lumsdon, A. E., MacDonald, G. K., Zarfl, C., & Reidy Liermann, C. (2015). An index-based framework for assessing patterns and trends in river fragmentation and flow regulation by global dams at multiple scales. *Environmental Research Letters*, 10, 015001. <https://doi.org/10.1088/1748-9326/10/1/015001>
- Hanegan, K. (2011). *Modeling evolution of the Wax Lake delta in Atchafalaya Bay, Louisiana*. Delft University of Technology.
- Hiatt, M., & Passalacqua, P. (2015). Hydrological connectivity in river deltas: The first-order importance of channel-island exchange. *Water Resources Research*, 51(4), 2264–2282. <https://doi.org/10.1002/2014WR016149>
- Hiatt, M., Sonke, W., Addink, E. A., van Dijk, W. M., van Kreveld, M., Ophelders, T., et al. (2020). Geometry and topology of estuary and braided river channel networks automatically extracted from topographic data. *Journal of Geophysical Research: Earth Surface*, 125, e2019JF005206. <https://doi.org/10.1029/2019JF005206>
- Hodges, B. R. (2015). Representing hydrodynamically important blocking features in coastal or riverine lidar topography. *Natural Hazards and Earth System Sciences*, 15, 1011–1023. <https://doi.org/10.5194/nhessd-3-1427-2015>
- Isikdogan, F., Bovik, A., & Passalacqua, P. (2015). Automatic channel network extraction from remotely sensed images by singularity analysis. *IEEE Geoscience and Remote Sensing Letters*, 12(11), 2218–2221. <https://doi.org/10.1109/LGRS.2015.2458898>
- Jiang, L., Madsen, H., & Bauer-Gottwein, P. (2019). Simultaneous calibration of multiple hydrodynamic model parameters using satellite altimetry observations of water surface elevation in the Songhua River. *Remote Sensing of Environment*, 225, 229–247. <https://doi.org/10.1016/j.rse.2019.03.014>
- Jin, S., Liu, Y., Fagherazzi, S., Mi, H., Qiao, G., Xu, W., et al. (2021). River body extraction from sentinel-2A/B MSI images based on an adaptive multi-scale region growth method. *Remote Sensing of Environment*, 255(8), 112297. <https://doi.org/10.1016/j.rse.2021.112297>
- Jones, J. E., & Davies, A. M. (2005). An intercomparison between finite difference and finite element (TELEMAC) approaches to modelling west coast of Britain tides. *Ocean Dynamics*, 55(3), 178–198. <https://doi.org/10.1007/s10236-005-0006-5>
- Kearney, W., & Fagherazzi, S. (2016). Salt marsh vegetation promotes efficient tidal channel networks. *Nature Communications*, 7, 12287. <https://doi.org/10.1038/ncomms12287>
- Kirwan, M. L., Temmerman, S., Skeehean, E. E., Guntenspergen, G. R., & Fagherazzi, S. (2016). Overestimation of marsh vulnerability to sea level rise. *Nature Climate Change*, 6(3), 253–260. <https://doi.org/10.1038/nclimate2909>
- Kleinhaus, M., van Kreveld, M., Ophelders, T., Sonke, W., Speckmann, B., & Verbeek, K. (2019). Computing representative networks for braided rivers. *Journal of Computational Geometry*, 10(1), 423–443. <https://doi.org/10.20382/jocg.v10i1a14>
- Lagrange, J. L. (1811). *Mécanique analytique*. Ve Courcier.

- Lesser, G. R., Roelvink, J. V., van Kester, J. T. M., & Stelling, G. S. (2004). Development and validation of a three-dimensional morphological model. *Coastal Engineering*, 51(8–9), 883–915. <https://doi.org/10.1016/j.coastaleng.2004.07.014>
- Li, Z., & Hodges, B. R. (2019). Model instability and channel connectivity for 2D coastal marsh simulations. *Environmental Fluid Mechanics*, 19, 1309–1338. <https://doi.org/10.1007/s10652-018-9623-7>
- Liao, T. H., Simard, M., Denbina, M., & Lamb, M. P. (2020). Monitoring water level change and seasonal vegetation change in the coastal wetlands of Louisiana using L-band time-series. *Remote Sensing*, 12(15). <https://doi.org/10.3390/RS12152351>
- Limaye, A. B. (2017). Extraction of multithread channel networks with a reduced-complexity flowmodel. *Journal of Geophysical Research: Earth Surface*, 122, 1972. <https://doi.org/10.1002/2016JF004175>
- List, J. H., Jaffe, B. E., Sallenger, A. H., & Hansen, M. E. (1997). Bathymetric comparisons adjacent to the Louisiana barrier islands: Processes of large-scale change. *Journal of Coastal Research*, 670–678.
- Liu, K., Chen, Q., Hu, K., Xu, K., & Twilley, R. R. (2018). Modeling hurricane-induced wetland-bay and bay-shelf sediment fluxes. *Coastal Engineering*, 135, 77–90. <https://doi.org/10.1016/j.coastaleng.2017.12.014>
- Mariotti, G., & Fagherazzi, S. (2012). Channels-tidal flat sediment exchange: The channel spillover mechanism. *Journal of Geophysical Research*, 117, C03032. <https://doi.org/10.1029/2011JC007378>
- Meselhe, E., Sadid, K., & Khadka, A. (2021). Sediment distribution, retention and morphodynamic analysis of a river-dominated deltaic system. *Water*, 13(10), 1341. <https://doi.org/10.3390/w13101341>
- Morris, J. T., Sundareswar, P. V., Nietch, C. T., Kjerfve, B., & Cahoon, D. R. (2002). Responses of coastal wetlands to rising sea level. *Ecology*, 83(10), 2869–2877. [https://doi.org/10.1890/0012-9658\(2002\)083\[2869:ROCWTR\]2.0.CO;2](https://doi.org/10.1890/0012-9658(2002)083[2869:ROCWTR]2.0.CO;2)
- Nijssen, B., O'Donnell, G. M., Lettenmaier, D. P., Lohmann, D., & Wood, E. F. (2001). Predicting the discharge of global rivers. *Journal of Climate*, 14(15), 3307–3323. [https://doi.org/10.1175/1520-0442\(2001\)014<3307:ptdogr>2.0.co;2](https://doi.org/10.1175/1520-0442(2001)014<3307:ptdogr>2.0.co;2)
- Olliver, E. A., Edmonds, D. A., & Shaw, J. B. (2020). Influence of floods, tides, and vegetation on sediment retention in Wax Lake Delta, Louisiana, USA. *Journal of Geophysical Research: Earth Surface*, 125(1), e2019JF005316. <https://doi.org/10.1029/2019JF005316>
- Passalacqua, P., Do Trung, T., Foufloula-Georgiou, E., Sapiro, G., & Dietrich, W. E. (2010). A geometric framework for channel network extraction from lidar: Nonlinear diffusion and geodesic paths. *Journal of Geophysical Research*, 115, F01002. <https://doi.org/10.1029/2009JF001254>
- Passalacqua, P., Lanzoni, S., Paola, C., & Rinaldo, A. (2013). Geomorphic signatures of deltaic processes and vegetation: The Ganges-Brahmaputra-Jamuna case study. *Journal of Geophysical Research: Earth Surface*, 118, 1838–1849. <https://doi.org/10.1002/jgrf.20128>
- Pitcher, L. H., Pavelsky, T. M., Smith, L. C., Moller, D. K., Altenau, E. H., Allen, G. H., et al (2019). AirSWOT InSAR mapping of surface water elevations and hydraulic gradients across the Yukon Flats Basin, Alaska. *Water Resources Research*, 55(2), 937–953. <https://doi.org/10.1029/2018WR023274>
- Redfield, A. C. (1972). Development of a new england salt marsh. *Ecological Monographs*, 42(2), 201–237. <https://doi.org/10.2307/1942263>
- Rinaldo, A., Fagherazzi, S., Lanzoni, S., Marani, M., & Dietrich, W. E. (1999). Tidal networks: 2. Watershed delineation and comparative network morphology. *Water Resources Research*, 35(12), 3905–3917. <https://doi.org/10.1029/1999WR900237>
- Roberts, H. H., DeLaune, R. D., White, J. R., Li, C., Sasser, C. E., Braud, D., & Khalil, S. (2015). Floods and cold front passages: Impacts on coastal marshes in a River diversion setting (Wax Lake delta area, Louisiana). *Journal of Coastal Research*, 31(5), 1057–1068. <https://doi.org/10.2112/JCOASTRES-D-14-54900173.1>
- Schuerch, M., Spencer, T., Temmerman, S., Kirwan, M. L., Wolff, C., Lincke, D., et al (2018). Future response of global coastal wetlands to sea-level rise. *Nature*, 561(13), 231–234. <https://doi.org/10.1038/s41586-018-0476-52>
- Schwenk, J., Piliouras, A., & Rowland, J. C. (2020). Determining flow directions in river channel networks using planform morphology and topology. *Earth Surf. Dynam*, 8(1), 87–102. <https://doi.org/10.5194/esurf-8-87-2020>
- Sethian, J. A. (1996). A fast marching level set method for monotonically advancing fronts. *Proceedings of the National Academy of Sciences*, 93(4), 1591–1595. <https://doi.org/10.1073/pnas.93.4.1591>
- Sethian, J. A., & Popovici, A. M. (1999). 3-D travelttime computation using the fast marching method. *Geophysics*, 64(2), 516–523. <https://doi.org/10.1190/1.1444558>
- Shaw, J. B., Mohrig, D., & Wagner, R. W. (2016). Flow patterns and morphology of a prograding river delta. *Journal Geophysical Research: Earth surface*, 121(2), 372–391. <https://doi.org/10.1002/2015JF003570>
- Shaw, J. B., Mohrig, D., & Whitman, S. K. (2013). The morphology and evolution of channels on the Wax Lake Delta, Louisiana, USA. *Journal of Geophysical Research: Earth Surface*, 118(3), 1562–1584. <https://doi.org/10.1002/jgrf.20123>
- Simard, M., Denbina, M. W., Jensen, D. J., & Lane, R. (2020). *Pre-Delta-X: Water levels across Wax Lake outlet, Atchafalaya basin, LA, USA, 2016*. ORNL DAAC. <https://doi.org/10.3334/ORNLDAAC/1801>
- Straatsma, M. W., & Baptist, M. J. (2008). Floodplain roughness parameterization using airborne laser scanning and spectral remote sensing. *Remote Sensing of Environment*, 112(3), 1062–1080. <https://doi.org/10.1016/j.rse.2007.07.012>
- Syvitski, J. P., Kettner, A. J., Overeem, I., Hutton, E. W., Hannon, M. T., Brakenridge, G. R., & Nicholls, R. J. (2009). Sinking deltas due to human activities. *Nature Geoscience*, 2(10), 681–686. <https://doi.org/10.1038/ngeo629>
- Thomas, N., Simard, M., Castañeda-Moya, E., Byrd, K. B., Windham-Myers, L., Bevington, A., & Twilley, R. (2019). High-resolution mapping of biomass and distribution of marsh and forested wetlands in southeastern coastal Louisiana. *International Journal of Applied Earth Observation and Geoinformation*, 80, 257–267. <https://doi.org/10.1016/j.jag.2019.03.013>
- Torres, R., & Styles, R. (2007). Effects of topographic structure on salt marsh currents. *Journal of Geophysical Research*, 112(F2), F02023. <https://doi.org/10.1029/2006JF000508>
- U.S. Geological Survey. (2016). *National water information system data available on the world wide web. USGS Water Data for the Nation*. accessed June 10 2012. Retrieved from <http://waterdata.usgs.gov/nwis/>
- Volp, N., van Prooijen, B., & Stelling, G. (2013). A finite volume approach for shallow water flow accounting for high-resolution bathymetry and roughness data. *Water Resources Research*, 49(7), 4126–4135. <https://doi.org/10.1002/wrcr.20324>
- Wang, B., Fringer, O., Giddings, S., & Fong, D. (2009). High-resolution simulations of a macrotidal estuary using SUNTANS. *Ocean Modelling*, 28(1–3), 167–192. <https://doi.org/10.1016/j.ocemod.2008.08.008>
- Wu, G., Shi, F., Kirby, J., Mieras, R., Liang, B., Li, H., & Shi, J. (2016). A pre-storage, subgrid model for simulating flooding and draining processes in salt marshes. *Coastal Engineering*, 108, 65–78. <https://doi.org/10.1016/j.coastaleng.2015.11.008>
- Yu, D., & Lane, S. (2011). Interactions between subgrid-scale resolution, feature representation and grid-scale resolution in flood inundation modelling. *Hydrological Processes*, 25, 36–53. <https://doi.org/10.1002/hyp.7813>
- Zhang, X., Fagherazzi, S., Leonardi, N., & Li, J. (2018). A positive feedback between sediment deposition and tidal prism may affect the morphodynamic evolution of tidal deltas. *Journal of Geophysical Research: Earth Surface*, 123(11), 2767–2783. <https://doi.org/10.1029/2018JF004639>
- Zhang, X., Leonardi, N., Donatelli, C., & Fagherazzi, S. (2020). Divergence of sediment fluxes triggered by sea-level rise will reshape coastal bays. *Geophysical Research Letters*, 47, e2020GL087862. <https://doi.org/10.1029/2020GL087862>